The quark propagator in the colour-spin locked phase

Marc Florian Marhauser

Diplomarbeit
TU Darmstadt
August 2006

Contents

1 Motivation

It is widely believed that quantum chromodynamics (QCD) is the correct quantum field theory of the strong interaction at energy scales available in recent experiments today. In the high energy limit QCD can be treated perturbatively, this treatment fails in the low and intermediate energy region. In these regions, many phenomena like confinement or chiral symmetry breaking occur.
For large baryon density and/or temperature quarks are believed to be no longer confined inside hadrons, because the hadrons have a big overlap and loose their individuality. The conjecture of such a quark-gluon plasma (QGP) came up in the 70s and we are quite certain that it existed a few microseconds after the big bang.
At the end of the 90s a phenomenon named "colour superconductivity" received a lot of attention. Colour superconductivity is the formation of Cooper pairs of quarks in the quark-gluon plasma and is assumed to occur in the region of low temperature and high baryon density. It had already been mentioned in 1975 [1]. First investigations of colour superconductivity in quark matter using perturbative one-gluon exchange interactions revealed only small diquark pairing gaps of about 1 MeV [2, 3]. However, the relevance of this state of matter had almost completely been ignored until the end of the 90s. More recent investigations employing low-energy models of QCD showed that the diquark pairing gaps can be as large as 100 MeV [4–7]. Because larger pairing gaps imply larger critical temperatures, the colour superconducting region could extend far into the temperature direction of the QCD phase diagram. An example of how a phase diagram of QCD could look like is shown in Fig. 1. Following these studies, more systematic approaches revealed a very rich phase structure of cold and dense quark matter [8–12]. This rich structure is possible because there are few constraints on the details of the Cooper pairing, allowing for a multitude of colour-superconducting phases.
The most prominent colour superconducting phases with large pairing gaps are the two-flavour colour superconducting phase (2SC) and the colour-flavour locked phase (CFL).

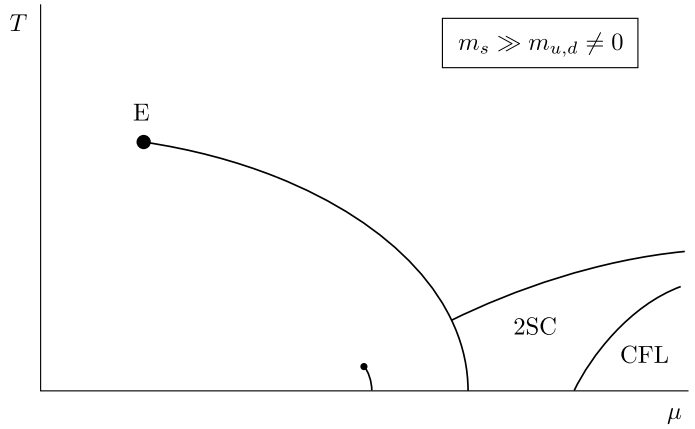

Figure 1: A schematic QCD phase diagram taken from [13]. T is the temperature and μ is the quark chemical potential. This phase diagram considers only two colour superconducting phases, the familiar "hadronic phase" in the lower left corner, where quarks and gluons are confined, and the QGP.

The CFL phase requires approximate $SU(3)$ flavour symmetry that is realized at rather large densities.
The environment in nature that could provide the conditions for colour superconductivity to occur are the interiors of compact stars, with temperatures clearly below 1 MeV and central densities exceeding the nuclear saturation density by about one order of magnitude. In general it is expected that colour-superconducting phases with large pairing gaps like 2SC or CFL are energetically favoured compared to spin-1 phases. For two reasons this might not be true in the case in the interior of a compact star. First, the densities might not be large enough to allow for the CFL phase to exist in this environment. Second, due to the requirement of charge and colour neutrality the star must obey, there may be no 2SC pairing in this environment [14]. This setting could allow for colour superconducting phases where quarks of different flavours pair independently. In these phases the Cooper pair of quarks carries spin 1.
Compact star phenomenology puts another constraint on the colour superconducting phase in its interior. To describe neutron star cooling data the colour superconducting phase should fullfill some constraints [15]: All excitation modes should be gapped, the smallest energy gap should be of the order of 10 - 100 keV and decrease with the density in the physically interesting region, which lies roughly between 300-500 MeV quark chemical potential μ. A possible spin-1 phase that could fulfill these requirements is the so called colour spin locked phase (CSL), that has also been found to be the most stable spin-1 phase at asymptotically high densities [16]. This phase has recently been investigated in an NJL type model [17] and promises to be a viable candidate for the phase of matter being realized in the interior of compact stars.
A recent version of the QCD phase diagram is shown in Fig. 2 (taken from [11]), where we can see the multitude of colour superconducting phases. The investigation in [11] neglected the CSL phase, that could exist in the region of temperature $T \lesssim 10$ MeV and chemical potential μ between 370 MeV and 440 MeV of the phase diagram in Fig. 2.
Much of the work done in the field of colour superconductivity has been done using models of the QCD interaction. This is sensible because a perturbative treatment of QCD fails in the interesting low temperature and intermediate density regime. A non-perturbative, model independent treatment of QCD is challenging, yet, inevitable to get reliable results. One of these non-perturbative approaches to QCD is possible within the framework of Dyson-Schwinger equations (DSEs). Dyson-Schwinger equations provide a set of coupled integral equations that are the quantum equations of motion of the Green functions of a quantum field theory. If they are solved completely, the whole dynamics of the theory under consideration is understood. For QCD there are, up to now, only solutions of subsets of the whole set of DSEs. The main problem to overcome is the non-linear coupling amongst the equations. To get to subsets of equations that can be solved, one uses truncations that decouple the desired subset of the DSEs. The solutions of these subsets of equations are of course only approximations to the solution of the full set, yet, they provided many intersting and usefull results. In our analysis, we will, except for medium modifications, decouple the quark from the gauge boson sector, assuming that the backreaction of quarks on the gauge boson sector is small.
This work is organised in the following form: First we will discuss the essentials of QCD needed here, along with the derivation of the Dyson-Schwinger equations for the quark

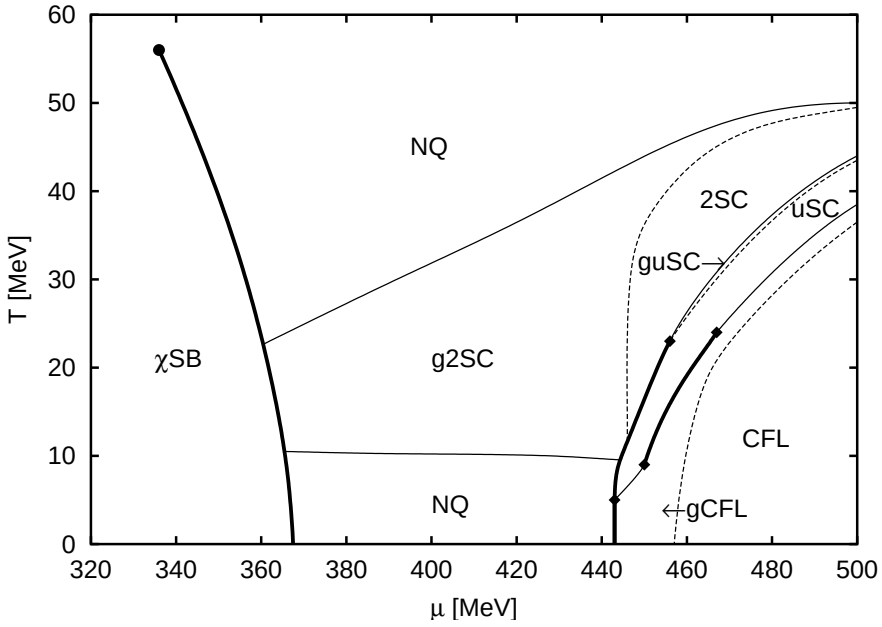

Figure 2: A part of the phase diagram of QCD. T is the temperature and μ is the quark chemical potential. Taken from [11].

propagator. We will continue with the introduction of the approximations being used and explain the Nambu-Gor'kov formalism that allows for an elegant treatment of colour superconductivity. A discussion of the colour-spin locked phase will conclude the introduction. The next two sections will focus on the solutions to the DSEs for the quark propagator. In the end we will focus on the resulting excitation spectra and finish with a summary of what we accomplished and an outlook.

2 Introduction

2.1 QCD essentials

The QCD partition function

A quantum field theory can be defined by a Lagrangian. The Lagrangian that we use to describe QCD in Euclidian space-time is given by

$$\mathcal{L}_{QCD} = \bar{\psi}\ (-\not{D} + m)\ \psi + \frac{1}{4} F^a_{\mu\nu} F^a_{\mu\nu}. \tag{1}$$

This Lagrangian is Lorentz invariant, invariant under local $SU(3)_c$ gauge transformations and renormalisable. Quarks are represented by Dirac spinors ψ and $\bar{\psi}$. Local gauge invariance is ensured by the covariant derivative in the fundamental representation of the gauge group $SU(3)_c$,

$$D_\mu = \partial_\mu + igA^a_\mu t^a, \tag{2}$$

where the t^a are the generators of the gauge group $SU(3)_c$ and A^a_μ are the gauge fields representing the gluons. g is the gauge coupling constant. The generators t^a of the gauge group obey the commutation relation

$$[t^a, t^b] = i f^{abc} t^c, \tag{3}$$

where f^{abc} are the structure constants of the gauge group. $F^a_{\mu\nu}$ is the gluon field strength tensor, given by

$$F^a_{\mu\nu} = \partial_\mu A^a_\nu - \partial_\nu A^a_\mu - g f^{abc} A^b_\mu A^c_\nu. \tag{4}$$

To quantise the theory it is advantageous to work in the path integral formalism. Therefore we introduce the partition function

$$Z[J, \eta, \bar{\eta}] = \int \mathcal{D}A \mathcal{D}\bar{\psi} \mathcal{D}\psi \exp\left[-S_{QCD} - \int d^4x \left(A^a_\mu J^a_\mu + \bar{\eta}\psi + \bar{\psi}\eta \right) \right], \tag{5}$$

where we used the abbreviation $S_{QCD} = \int d^4x\ \mathcal{L}_{QCD}$ for the QCD action. $J^a_\mu, \bar{\eta}$ and η are external source terms for the gauge fields, quark and adjoint quark fields respectively. $\bar{\eta}$ and η are Grassmann valued.

Gauge fixing

The quantisation of a gauge theory can be complicated due to gauge invariance. By performing the path integral, we integrate over all possible configurations of Dirac and gauge fields. This means a multiple counting of physically equivalent configurations, namely those that are connected by a gauge transformation. The integration thus generates an infinite constant - the volume of the gauge group - that can be absorbed in the normalisation of the partition function.
Due to gauge freedom we cannot define a perturbative gauge field propagator. This is

a consequence of the zero eigenmodes that exist in the quadratic part of the gauge field Lagrangian, which therefore cannot be inverted. The troublesome modes are the modes that are gauge equivalent to $A^a_\mu = 0$.
To define a gauge field propagator we have to fix a gauge. This is preferably done via the Faddeev-Popov procedure, whose main idea is to separate the integration over the gauge fields in an integration over different gauge orbits and an integration along those orbits. In practice this is done by inserting the identity

$$1 = \int \mathcal{D}\alpha \; \delta\left[G(A^\alpha)\right] \mathrm{Det}\left[\frac{\delta G(A^\alpha)}{\delta \alpha}\right] \tag{6}$$

into the partition function, where $G(A^\alpha)$ is a function that encodes the gauge fixing condition and A^α is the gauge field A, transformed through a finite gauge transformation:

$$(A^\alpha)^a_\mu t^a = e^{-i\alpha^a t^a}\left[A^b_\mu t^b + \frac{i}{g}\partial_\mu\right] e^{i\alpha^c t^c}. \tag{7}$$

Using the gauge fixing condition

$$G(A) = \partial_\mu A^a_\mu(x) - \omega^a(x), \tag{8}$$

where ω is an arbitrary function, the functional determinant in Eq. (6) takes the explicit form

$$\mathrm{Det}\left[\frac{\delta G(A^\alpha)}{\delta \alpha}\right] = \mathrm{Det}\left[-\partial_\mu D^{ab}_\mu\right], \tag{9}$$

where $D^{ab}_\mu = \partial_\mu \delta^{ab} + g f^{abc} A^c_\mu$ is the covariant derivative in the adjoint representation. In contrast to abelian gauge theories - where the functional determinant is independent of A and can thus be absorbed in the normalisation of the partition function - the determinant introduces new terms in the Lagrangian. Faddeev and Popov wrote the functional determinant as a functional integral over a set of anticommuting fields in the adjoint representation

$$\mathrm{Det}\left[-\partial_\mu D^{ab}_\mu\right] = \int \mathcal{D}c\mathcal{D}\bar{c} \exp\left[i\int d^4x \; \bar{c}(-\partial_\mu D^{ab}_\mu)c\right]. \tag{10}$$

The fields c and $\bar{c}$, called "Faddeev-Popov ghosts", are scalar Grassmannian fields that violate the spin-statistic theorem and thus cannot be asymptotic states. However they serve as negative degrees of freedom that cancel unphysical longitudinal polarisations of the gluons and are necessary to preserve unitarity.
Eventually we want to write the gauge fixing term $\delta\left[G(A^\alpha)\right]$ as a Gaussian integral. Together with the ghost field action this gives the gauge fixing action term

$$S_{gf} = \int d^4x \left(\frac{(\partial_\mu A^a_\mu)^2}{2\xi} - i\bar{c}(-\partial_\mu D^{ab}_\mu)c\right), \tag{11}$$

that has to be added to the QCD action in the partition function. ξ is a freely adjustable gauge parameter. We will work in Landau gauge:

$$G(A) = \partial_\mu A^a_\mu(x) = 0, \qquad \xi = 0. \tag{12}$$

$\xi = 0$ enforces an infinite weight in the Gaussian integral and thereby restricts even quantum fluctuations to $\partial_\mu A_\mu = 0$. The partition function is finally given by

$$Z[J,\eta,\bar{\eta},\sigma,\bar{\sigma}] = \tag{13}$$
$$\mathcal{N}\int \mathcal{D}A\mathcal{D}\bar{\psi}\mathcal{D}\psi\mathcal{D}\bar{c}\mathcal{D}c \exp\left[-S_{QCD} - S_{gf} + \int d^4x \left(A^a_\mu J^a_\mu + \bar{\eta}\psi + \bar{\psi}\eta + \bar{\sigma}c + \bar{c}\sigma\right)\right],$$

where $\mathcal{N}$ is the normalisation constant of the partition function. A finite chemical potential μ for the quark current is practically introduced as a Lagrange multiplier [18]:

$$S_{QCD} \to S_{QCD} - \int d^4x\ \bar{\psi}\mu\gamma_4\psi. \tag{14}$$

Renormalisation

The theory defined in Eq. (13) is not renormalised, therefore loop integrals will give divergent results. To overcome this we need to renormalise the theory by rescaling the fields:

$$A^a_\mu \to \sqrt{Z_3}A^a_\mu\ ,\ \bar{c}^a c^b \to \tilde{Z}_3 \bar{c}^a c^b\ ,\ \bar{\psi}\psi \to Z_2\bar{\psi}\psi\ ,\ g \to Z_g g\ ,\ \xi \to Z_\xi \xi. \tag{15}$$

Note that in Landau gauge the gauge paramter ξ does not get renormalised. The five independent renormalisation constants $Z_3, \tilde{Z}_3, Z_2, Z_g, Z_\xi$ depend upon the regularisation scheme. There are five additional renormalisation constants, $Z_1, \tilde{Z}_1, Z_{1F}, Z_4, \tilde{Z}_4$, that are related to the ones in Eq. (15) via Slavnov-Taylor identities:

$$Z_1 = Z_g Z_3^{3/2}\ ,\ \tilde{Z}_1 = Z_g \tilde{Z}_3 Z_3^{1/2}\ ,\ Z_{1F} = Z_g Z_3^{1/2} Z_2\ ,\ Z_4 = Z_G^2 Z_3^2\ ,\ \tilde{Z}_4 = Z_g^2 \tilde{Z}_3^2. \tag{16}$$

These renormalisation constants are needed in the renormalisation of the vertex.

2.2 Dyson-Schwinger equations

Dyson-Schwinger equations (DSEs) provide an excellent method to approach continuum QCD in the strong coupling regime. DSEs are a nonperturbative method of analysing a quantum field theory. The DSEs are an enumerable infinity of coupled integral equations and their solutions are the n-point Green functions of the theory.
In this section, without allowing for colour superconductivity, we are going to derive the QCD gap equation [19] which is a basis for studying dynamical symmetry breaking in QCD. The QCD gap equation is a good example of a Dyson-Schwinger equation (DSE), since it shows all the characteristics of a DSE: its solution is a 2-point function (the quark propagator) while its kernel involves higher n-point, here $n = 3$, functions; in our case these are the gluon propagator, a 2-point function and the quark-gluon vertex, a 3-point function.
The coupling between equations, i.e., that the equation for a given m-point function always involves at least one n-point function with n > m, requires a truncation of the tower of DSEs in order to solve the set of equations. One systematic and familiar truncation is a weak coupling expansion that reproduces perturbation theory. We will not persue this path, instead we will use the quenched abelian approximation, that decouples the quark DSE from the rest of the DSEs.

The unrenormalised DSE

For clarity in our notation we will first derive the unrenormalised DSE and later renormalise it.
The main idea behind Dyson-Schwinger equations is the observation that the integral of a total derivative vanishes, see e.g. [20]. To get the quark Dyson-Schwinger equation we take the derivative of the partition function with respect to $\bar{\psi}$. For ease of notation, we will collect all source terms in $S_{source} = \int d^4x \left(A^a_\mu J^a_\mu + \bar{\eta}\psi + \bar{\psi}\eta + \bar{\sigma}c + \bar{c}\sigma \right)$.

$$\begin{aligned}
0 &= \int \mathcal{D}A\mathcal{D}\bar{\psi}\mathcal{D}\psi\mathcal{D}\bar{c}\mathcal{D}c \; \frac{\delta}{\delta\bar{\psi}(x)} \exp\left[-S_{QCD} - S_{gf} + S_{source}\right] \\
&= \int \mathcal{D}A\mathcal{D}\bar{\psi}\mathcal{D}\psi\mathcal{D}\bar{c}\mathcal{D}c \left[\frac{\delta S_{QCD}}{\delta\bar{\psi}(x)} + \eta(x)\right] \exp\left[-S_{QCD} - S_{gf} + S_{source}\right] \\
&= \left[\frac{\delta S_{QCD}}{\delta\bar{\psi}(x)} \left(\frac{\delta}{i\delta J^\mu_A(x)}, \frac{\delta}{i\delta\bar{\eta}(x)}, -\frac{\delta}{i\delta\eta(x)}\right) + \eta(x)\right] Z(J,\eta,\bar{\eta}) \qquad (17) \\
&= \left[\eta(x) + \left(\not{\partial} - \gamma_4\mu - m + ig\gamma^\mu t_a \frac{\delta}{i\delta J^a_\mu(x)}\right) \frac{\delta}{i\delta\bar{\eta}(x)}\right] Z(J,\eta,\bar{\eta}).
\end{aligned}$$

This form of the DSE is quite unwieldy. The steps necessary to transform it into a more concise form are given in appendix B, here we only quote the result:

$$\begin{aligned}
\delta^4(x-y) &= \left(\not{\partial}_x - \gamma_4\mu - m\right) S(x,y) + \\
&\quad \int d^4z d^4w d^4v \;\; ig\gamma^\mu t_a D^{\mu\nu}_{ab}(x,z) S(x,w) \Gamma^b_\nu(w,v,z) S(v,y) \qquad (18) \\
&= \int d^4v \left[\left(\not{\partial}_x - \gamma_4\mu - m\right) \delta^4(x-v) + \right. \\
&\quad \left. ig \int d^4w d^4z \;\; \gamma^\mu t_a D^{\mu\nu}_{ab}(x,z) S(x,w) \Gamma^b_\nu(w,v,z)\right] S(v,y). \qquad (19)
\end{aligned}$$

We introduced the full quark propagator $S(x,y)$, the full gluon propagator $D^{\mu\nu}_{ab}(x,y)$ and the full quark-gluon vertex $\Gamma^a_\mu(x,y,z)$. Their definition is also given in appendix B.
Defining the proper quark self-energy

$$\Sigma(x,y) = ig \int d^4w d^4z \; \gamma^\mu t_a D^{\mu\nu}_{ab}(x,z) S(x,w) \Gamma^b_\nu(w,v,z), \qquad (20)$$

the quark DSE takes a simple form:

$$\delta^4(x-y) = \int d^4v \left[\left(\not{\partial}_x - \gamma_4\mu - m\right) \delta^4(x-v) + \Sigma(x,v)\right] S(v,y). \qquad (21)$$

The property of Green functions to be translationally invariant in the absence of external sources can be used to Fourier transform the QCD gap equation, Eq. (18), into momentum space. After some simple algebraic manipulations we get

$$\begin{aligned}
S^{-1}(p) &= S_0^{-1}(p) + \Sigma(p), \qquad (22) \\
\Sigma(p) &= -g^2 \int \frac{d^4q}{(2\pi)^4} \; \Gamma^\mu_{0\,a} \; S(q) \; \Gamma^\nu_b(p,q) \; D^{\mu\nu}_{ab}(p-q). \qquad (23)
\end{aligned}$$

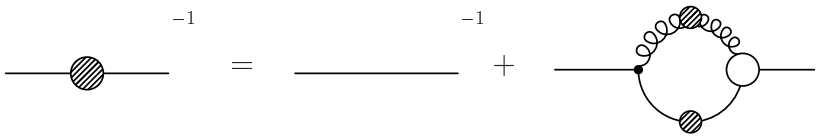

Figure 3: The diagrammatic Dyson-Schwinger equation for the quark propagator. White circles represent full vertices, bare vertices are represented by black dots. Bare quark propagators are shown as black lines, full quark propagators have a shaded circle. The curly line with a shaded circle is the full gluon propagator.

This equation is graphically shown in Fig. 3. We will mainly deal with this equation. Provided we know the vertex $\Gamma^\mu_a(p,q)$ and the gluon propagator $D^{ab}_{\mu\nu}(p-q)$, we can compute the quark propagator. The derivation of the Dyson-Schwinger equation for the quark propagator in the CSL phase is completely analogue to the one in this section, we will do this later.

The renormalised DSE

By renormalising the theory, several quantities in the gap equation undergo changes, i.e. they are multiplied by renormalisation constants. As we can see from Eq. (15) the inverse bare propagator S_0^{-1} acquires a factor of Z_2. The selfenergy receives a factor of $Z_g Z_2 \sqrt{Z_3}$ from the bare vertex, this factor is just Z_{1F} in Eq. (16). Thus the renormalised quark DSE is:

$$S^{-1}(p) = Z_2 S_0^{-1}(p) + Z_{1F}\Sigma(p), \tag{24}$$

$$\Sigma(p) = -g^2 \int \frac{d^4q}{(2\pi)^4}\, \Gamma^\mu_{0\,a}\; S(q)\; \Gamma^\mu_b(p,q)\; D^{\mu\nu}_{ab}(p-q). \tag{25}$$

Solving the QCD gap equation

To solve the QCD gap equation, Eq. (24), we will make use of the quenched abelian approximation. This decouples the QCD gap equation from the infinite tower of DSEs. The only unknown is then the full quark propagator. For simplicity let us neglect the chemical potential for a moment. A Lorentz invariant parametrisation of the full quark propagator S is then given by

$$S(p) = \frac{Z(p^2,\nu)}{i\not{p} + M(p^2)}. \tag{26}$$

$\not{p} \equiv p_\mu\, \gamma_\mu$ is defined according to the Feynmann convention. The Lorentz scalars $Z(p^2,\nu)$ and $M(p^2)$ are referred to as the quark wave function renormalisation and the dressed quark mass-function respectively. ν is the renormalisation point, that $M(p^2)$ is independent of.
Inserting this parametrisation into the QCD gap equation, Eq. (24), we can trace out scalar equations for the quark wave function renormalisation and the dressed quark mass-function. This scheme will be employed throughout this work, however, in a more elaborate fashion.

2.3 Truncations

As mentioned at the beginning of the previous section, the DSE for a n-point Green function always depends on at least one m-point function, with m > n. An example, that we presented above, is the QCD gap equation, Eq. (25) ($n = 2$), it is coupled to the quark-gluon vertex ($m = 3$). Another Green function the QCD gap equation is coupled to is the gluon propagator, a two-point function.
Because the gluon propagator and the quark-gluon vertex satisfy their own DSEs, they also couple the QCD gap equation to other equations of the infinite tower of equations. Therefore, we have to know the values of these Green functions for all values of their momentum arguments. Provided that this is known, the quark propagator can be determined from Eq. (24).
In Landau gauge, that we will be working in, these Green functions were investigated for the chirally broken phase at zero chemical potential by DSE studies and by lattice QCD calculations, see *e.g.* [21, 22]. In Landau gauge, the vacuum gluon propagator is parameterised by a single dressing function $Z(k^2)$,

$$D^{ab}_{\mu\nu}(k^2) = \delta^{ab}\left(\delta_{\mu\nu} - \frac{k_\mu k_\nu}{k^2}\right)\frac{Z(k^2)}{k^2}. \tag{27}$$

$k^2 = (p-q)^2$ is the squared difference between the external momentum p and the loop momentum q in the QCD gap equation, Eq.(24).
For the quark-gluon vertex we will use an approximation that separates the vertex into its tree-level form and a multiplicative dressing function.

$$\Gamma^a_\mu(p,q) = i\Gamma((p-q)^2)\gamma_\mu\frac{\lambda^a}{2}. \tag{28}$$

The unknown dressing function $\Gamma(k^2)$ encodes the non-perturbative behaviour of QCD and it has been chosen such that the quark propagator is multiplicatively renormalisable and in agreement with perturbation theory in the ultraviolet [21]. It can also be determined from quenched lattice QCD calculations of the quark and gluon propagator [22]. The dressing functions enter the QCD gap equation only in terms of their product

$$\alpha_s(k^2) = \frac{Z_{1F}}{Z_2^2}\frac{g^2}{4\pi}Z(k^2)\Gamma(k^2). \tag{29}$$

Here Z_{1F} is the quark-gluon coupling and Z_2 the quark-wave-function renormalisation constant, respectively. We will call $\alpha_s(k^2)$ the effective strong running coupling because, especially in the framework of DSEs, it is a possible non-perturbative extension of the strong coupling into the infrared.
Throughout this work we will use two differnt effective strong running couplings. One is obtained from DSE studies of the Yang-Mills sector of QCD [21], we will call it $\alpha_I(k^2)$. The effective strong running coupling extracted from lattice QCD simulations [22] will be named $\alpha_{II}(k^2)$. The two effective strong running couplings as a function of k^2 are shown in Fig. 4. Their infrared behaviour is quite different. Also their coupling strength differs significantly. The effective strong running coupling $\alpha_I(k^2)$ can be viewed as a lower bound to the coupling strength, whereas α_{II} is a good upper bound to the coupling strength.

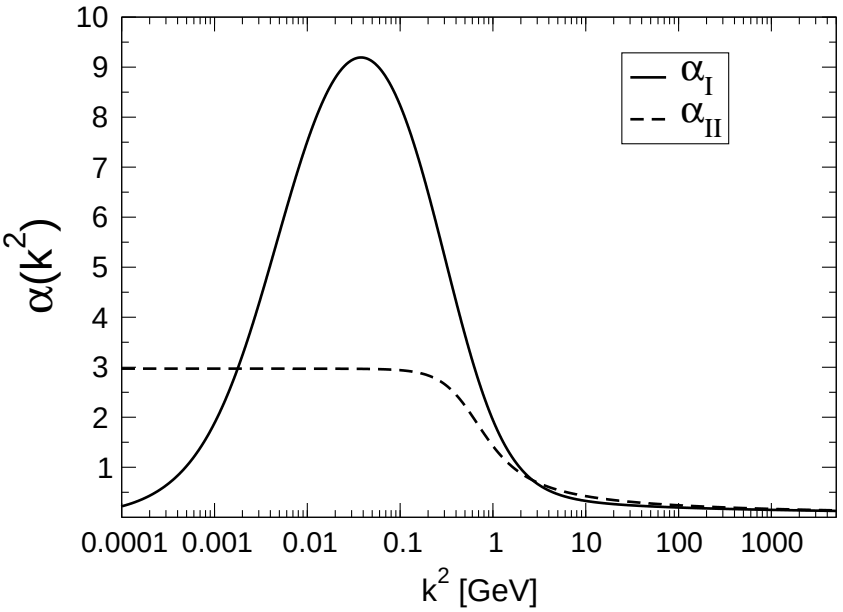

Figure 4: The effective strong running couplings $\alpha_I(k^2)$ and $\alpha_{II}(k^2)$ as a function of k^2

α_{II} is parametrised such that the dressed quark mass function $M(p^2)$ (cf. Eq. (26)) is compatible with the results of lattice QCD calculations. α_I gives a dressed quark mass function $M(p^2)$ that is by a factor 3 smaller in the infrared, than $M(p^2)$ calculated using α_{II}. We can interpret this as a sign of stronger breaking of chiral symmetry by α_{II}.
For a non-vanishing quark chemical potential we expect the gluon propagator and the quark-gluon vertex to be modified compared to the vacuum. To account for the medium effects we will include damping and screening of the gluons by particle-hole excitations. In practice we add the in-medium polarisation tensor with 'bare' quark propagators to the inverse gluon propagator [23]. This is not self-consistent and needs to be investigated in further studies. Nevertheless, the resulting quark DSE turns out to be a generalisation of the so called "hard dense loop" (HDL) resummation scheme. The important difference is that the infrared behaviour of the gluon propagator and quark-gluon vertex is non-trivial. The HDL approximation is an extension of perturbation theory and takes medium modifications into account, a detailed treatment can be found in the literature, see e.g. [24]. The general idea is that the chemical potential μ introduces a new, "hard" scale that separates the scale of momenta. Momenta much smaller than μ are "soft". Calculating loop diagrams in this scheme one uses the assumption that internal momenta in loop diagrams are exclusively "hard", i.e. the absolute value of the spatial momentum is approximated by the chemical potential μ.
The name "HDL resummation scheme" arises from the observation that the DSE, e.g. for the gluon propagator, is given by (neglecting Dirac and colour indices)

$$D = D_0 - D_0 \Pi D. \tag{30}$$

Here D denotes the full gluon propagator, D_0 is the bare gluon propagator and Π the gluon selfenergy. By iterating this equation it becomes apparent that it stands for an infinite series of diagrams. Thus the solution is a *resummed* propagator, where the selfenergy Π,

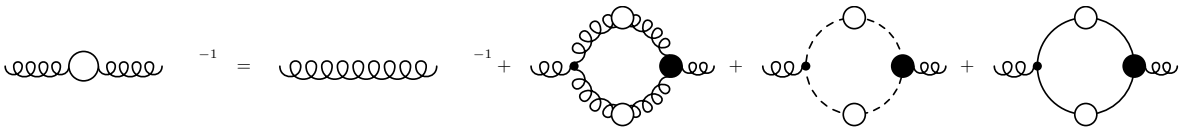

Figure 5: Diagrammatical representation of the approximate DSE for the gluon propagator used in [21]. Lines with empty circles denote full propagators, whereas lines without a circle denote bare propagators. Dots represent bare vertices, black circles denote full vertices. Curly lines represent gluons, dashed lines ghosts and regular lines quarks.

that is being resummed is computed using the *HDL* approximation.
To include the medium modifications we start from the approximate DSE for the gluon propagator in Landau gauge that was used in [21] to calculate $\alpha_I(k^2)$. It is shown diagrammatically in Fig. 5. In the approximation two diagrams involving more than one loop were neglected, because their influence is expected to be rather weak, however, they lead to modfications in the intermediate momentum region. This DSE was solved in the vacuum. We would like to solve it approximately in the medium. Going from the vacuum to the medium, we assume that the main modification originates from the last term in the DSE in Fig. 5, where the loop involves quarks. We approximate the first three terms to be equal to the corresponding terms in the vacuum and the vertices are assumed to remain unchanged in the medium.
The final step is to add and subtract the last term of the gluon DSE in Fig. 5, evaluated in the vacuum, and rearrange the diagrams. This is shown in Fig. (6). The first four terms on the right hand side are precisely the full gluon propagator in the vacuum obtained in the approximation used in [21]. We will call the remaining two term the renormalised medium polarisation tensor.

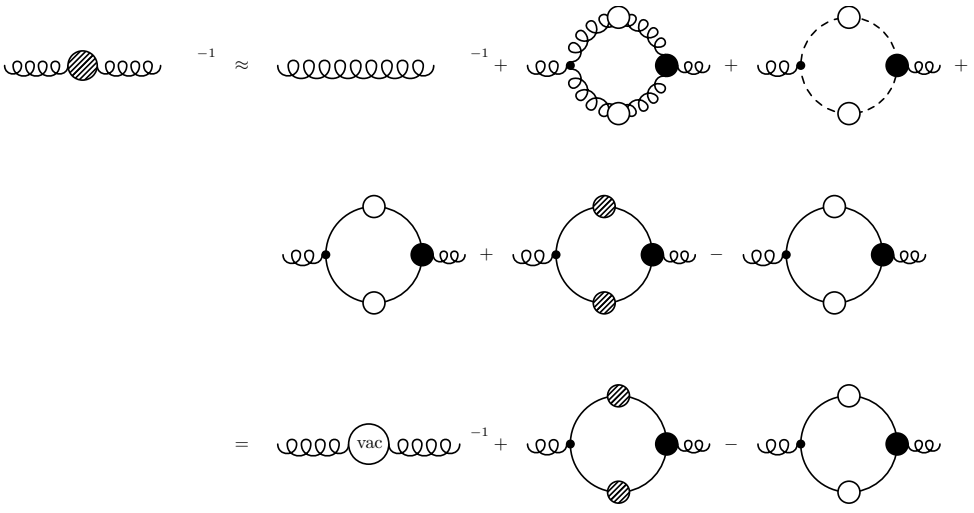

Figure 6: Diagrammatical representation of the DSE for the gluon propagator in medium. Lines with empty circles denote full propagators, whereas lines without a circle denote bare propagators, in the vacuum. Lines with shaded circles represent full propagators in the medium. Dots represent bare vertices, black circles denote full vertices in the vacuum.

The renormalised medium polarisation tensor is then given by

$$\Pi^{\mathrm{med}\,ab}_{\mu\nu}(p) = \quad \frac{1}{2} Z_{1F} \int \frac{d^4q}{(2\pi)^4} \mathrm{Tr}_{D,c,f} \left(\left[\Gamma^{(0)a}_{\mu} \mathcal{S}(q) \Gamma^{b}_{\nu}(q, p-q) \mathcal{S}(p-q) \right] - [\ldots]_{\mu=0} \right) \quad (31)$$

$\mathrm{Tr}_{D,c,f}$ denotes traces in Dirac, colour and flavour space. For the first part we employ the approximation of vanishing quark self-energies and the vertex (29). Then this expression can be straightforwardly reduced to

$$\begin{aligned} \Pi^{\mathrm{med}\,ab}_{\mu\nu}(p) &= -\frac{Z_{1F}}{Z_2^2} \frac{g^2 N_f}{2} \delta^{ab} \Gamma(p^2) \int \frac{d^4q}{(2\pi)^4} \mathrm{Tr}_D \left([\gamma_\mu S_0(q) \gamma_\nu S_0(p-q)] - [\ldots]_{\mu=0} \right) \\ &= -\delta^{ab} \frac{2\pi N_f \alpha_s(p^2)}{Z(p^2)} \int \frac{d^4q}{(2\pi)^4} \mathrm{Tr}_D \left([\gamma_\mu S_0(q) \gamma_\nu S_0(p-q)] - [\ldots]_{\mu=0} \right). \quad (32) \end{aligned}$$

The medium polarisation tensor can be decomposed according to its tensor structure. This decomposition can be done with the help of projectors on the spatially transverse and longitudinal subspace orthogonal to p^μ,

$$P^T_{44} = P^T_{i4} = P^T_{4i} = 0, \quad P^T_{ij} = \delta_{ij} - \frac{p_i p_j}{\vec{p}^2}, \quad (33)$$

and

$$P^L_{\mu\nu} = (\delta_{\mu\nu} - p_\mu p_\nu / p^2) - P^T_{\mu\nu}, \quad (34)$$

respectively. Then two functions, $G(|\vec{p}|, p_4)$ and $F(|\vec{p}|, p_4)$, are sufficient to write the medium polarisation tensor in the form

$$Z(p^2) \Pi^{ab}_{\mu\nu}(p) = G(p) \delta^{ab} P^T_{\mu\nu} + F(p) \delta^{ab} P^L_{\mu\nu}. \quad (35)$$

The evaluation of these functions is well known perturbatively. Compared to the perturbative result only the coupling constant is replaced by the running coupling. For small external momenta the result is

$$G(|\vec{p}|, p_4) = m^2(p^2) \frac{ip_4}{|\vec{p}|} \left[\left(1 - \left(\frac{ip_4}{|\vec{p}|} \right)^2 \right) Q\left(\frac{ip_4}{|\vec{p}|} \right) + \frac{ip_4}{|\vec{p}|} \right], \quad (36)$$

$$F(|\vec{p}|, p_4) = 2m^2(p^2) \frac{p_4^2 + \vec{p}^2}{\vec{p}^2} \left[1 - \frac{ip_4}{|\vec{p}|} Q\left(\frac{ip_4}{|\vec{p}|} \right) \right], \quad (37)$$

with $Q(x) = \frac{1}{2} \ln \frac{x+1}{x-1}$ and

$$m^2(p^2) = N_f \alpha_s(p^2) \mu^2 / \pi. \quad (38)$$

$m(p^2)$ can be interpreted as an effective mass of the gluons. Eventually the inverse medium gluon propagator is given by adding the medium polarisation tensor to the inverse vacuum gluon propagator. The medium gluon propagator is then

$$\begin{aligned} D^{ab}_{\mu\nu}(p) &\approx \left(D^{vac\,-1}_{\mu\nu}(p^2) + \Pi^{\mathrm{med}\,ab}_{\mu\nu}(p) \right)^{-1} \\ &= \delta^{ab} \left(\frac{p^2}{p^2 + G(p)} P^T_{\mu\nu} + \frac{p^2}{p^2 + F(p)} P^L_{\mu\nu} \right) \frac{Z(p^2)}{p^2}. \quad (39) \end{aligned}$$

Taking into account this form of the in-medium polarisation, Debye screening and Landau damping are included, similar to the HDL approximation. It becomes evident that these phenomena have a non-perturbative origin and require the knowledge of the infrared behaviour of Green functions, in particular of $\alpha_s(k^2)$. This procedure could be refined by using dressed quark propagators instead of bare quark propagators when solving Eq. (32).

2.4 Colour superconductivity

In systems of fermions with equal Fermi energies and an attractive interaction, according to Cooper's theorem [25], a formation of Cooper pairs occurs. In ordinary metallic superconductors the microscopic interaction between electrons is repulsive, yet, the phonon exchange in superconductors renders the interaction attractive.
The microscopic interaction between quarks is already attractive in certain channels. For sufficiently cold and dense quark matter, where quarks are presumeably deconfined, this interaction is given predominantly by one-gluon exchange. The interaction can also be given by instanton inspired models, also NJL type interactions are possible. Then the quarks at their Fermi surface rearrange in order to form a ground state characterised by the existence of quark Cooper pairs [2–4].
In our analysis we expect only the three lightest flavours to be colour-superconducting, even though the CSL phase we are going to consider, is flavour independent. This assumption is justified since the interesting regime of the quark chemical potential never exceeds the charm-quark mass. Therefore charm, bottom and top quarks are too heavy, even at low, non-zero temperatures their abundance is exponentially suppressed.

Diquark condensates

A diquark condensate, characterising a colour-superconducting state as its order parameter is defined as the expectation value

$$\left\langle \psi^T C\mathcal{O}\psi \right\rangle , \tag{40}$$

where ψ is a quark field operator with spin, flavour and colour degrees of freedom. $C = \gamma_2\gamma_4$ is the charge conjugation operator. ψ^T is the transposed quark field operator. The operator $\mathcal{O}$ acts in Dirac, colour and flavour space, and can be expressed by a sum of elements of the form

$$\mathcal{O} = \mathcal{O}_{Dirac} \otimes \mathcal{O}_{colour} \otimes \mathcal{O}_{flavour}. \tag{41}$$

The only constraint on the operator $\mathcal{O}$ is given by the Pauli principle, that manifests itself in the anticommutation relations of the quark field operators:

$$\psi^T C\mathcal{O}\psi = (C\mathcal{O})_{ij}\psi_i\psi_j = -(C\mathcal{O})_{ij}\psi_j\psi_i = -\psi^T(C\mathcal{O})^T\psi, \tag{42}$$

thus the operator $\mathcal{CO}$ has to be totally antisymmetric. Equivalently we can require the condition $\mathcal{O}^T = C\mathcal{O}C^{-1}$. Because there are many operators in Dirac, colour and flavour space, one can see that there is a multitude of different ways that one can build up

	antisymmetric	symmetric
Dirac	$\gamma_\mu,\ \sigma_{\mu\nu}, p_\mu,$	$\gamma_5,\ 1,\ \gamma_\mu\gamma_5,\ \gamma_\mu p_\mu$
$SU(3)$	$\lambda_2,\ \lambda_5,\ \lambda_7$	$\lambda_1,\ \lambda_3,\ \lambda_4,\ \lambda_6,\ \lambda_8$

Table 1: Symmetry properties of Dirac operators and the generators of $SU(3)$ under transposition. λ_i denotes Gell-Mann matrices.

the operator $\mathcal{O}$ in Eq. (40). The operators that can be used to construct $\mathcal{O}$ and their behaviour under transposition is is listed in Table (1). The $SU(3)$ operators act in colour space. Since we are going to consider only one-flavour superconductors we assume that the operator in flavour space is the identity operator: $\mathcal{O}_{flavour} = 1$. In the operator $\mathcal{O}$ also derivativelike operators can appear.
A finite diquark condensate will lead to a dynamical symmetry breaking, which equivalently characterises the phase. This means that all quantities arising in the treatment of the colour-superconducting phase have to respect the symmetries, the diquark condensate respects.

Derivation of the gap equation

We are going to treat colour superconductivity within the Nambu-Gor'kov formalism [26]. This is a convenient way of introducing diquark condensates. First we introduce bispinors

$$\Psi = \begin{pmatrix} \psi \\ \psi_c \end{pmatrix}, \quad \bar{\Psi} = \left(\bar{\psi}, \bar{\psi}_c\right), \tag{43}$$

where the charge conjugate spinors ψ_c and $\bar{\psi}_c$ are defined by

$$\psi_c = C\bar{\psi}^T, \quad \bar{\psi}_c = \psi^T C, \qquad C = \gamma_2\gamma_4. \tag{44}$$

We will exploit the observation that the action is scalar, $S = S^T$, to write the fermionic part of the QCD action in terms of bispinors.

$$\begin{aligned} S_{QCD} &= S_{QCD}^T = \left(\int d^4x\ \bar{\psi}\left(-\not{D} + \mu\gamma^4 + m\right)\psi\right)^T \\ &= -\int d^4x\ \psi^T\left(-\overleftarrow{\not{D}}^T + \mu\gamma^{4\,T} + m\right)\bar{\psi}^T \\ &= \int d^4x\ \psi^T C\left(-\not{D}_c - \mu\gamma^4 + m\right)C\bar{\psi}^T \\ &= \int d^4x\ \bar{\psi}_c\left(-\not{D}_c - \mu\gamma^4 + m\right)\psi_c, \end{aligned} \tag{45}$$

where $\not{D}_c = \gamma\cdot(\partial - igA^a\lambda^{aT})$ is the charge conjugate covariant derivative in the fundamental representation of the gauge group $SU(3)_c$. It is now possible to write the fermionic part of the QCD action in Nambu-Gor'kov space as

$$S_{QCD,F} = \frac{1}{2}\int d^4x\ \bar{\Psi}(x)\,\mathcal{D}_0^{-1}\,\Psi(x)\ , \tag{46}$$

where we introduced

$$\mathcal{D}_0^{-1} \equiv \begin{pmatrix} D_0^+ & 0 \\ 0 & D_0^- \end{pmatrix} \equiv \begin{pmatrix} -\not{D} + \mu\gamma_4 + m_0 & 0 \\ 0 & -\not{D}_c - \mu\gamma_4 + m_0 \end{pmatrix}, \tag{47}$$

The factor 1/2 in Eq. (46) compensates the doubling of degrees of freedom in Nambu-Gor'kov space. The derivation of the Dyson-Schwinger equation for the quark propagator is completely analogous to the derivation without colour superconductivity, we simply have to incorporate the Nambu-Gor'kov structure. The DSE for the quark propagator is given by

$$\mathcal{S}^{-1} = Z_2 \mathcal{S}_0^{-1} + Z_{1F}\Sigma. \tag{48}$$

In Nambu-Gor'kov space the structure is of the same form as the QCD gap equation, which should be expected. The Fourier transformed bare quark propagator in Nambu-Gor'kov space is

$$\mathcal{S}_0(p) = \begin{pmatrix} S_0^+ & 0 \\ 0 & S_0^- \end{pmatrix} \equiv \begin{pmatrix} (-i\vec{\not{p}} - i\not{\omega}_p + m_0)^{-1} & 0 \\ 0 & (-i\vec{\not{p}} - i\not{\omega}_p^* + m_0)^{-1} \end{pmatrix} \tag{49}$$

where we introduced the notation

$$\vec{\not{p}} \equiv \vec{p}\cdot\vec{\gamma}, \quad \not{\omega}_p \equiv \omega_p\gamma_4 \equiv (p_4 + i\mu)\gamma_4. \tag{50}$$

The selfenergy has more structure than in non-superconducting matter. We denote its components by

$$\Sigma \equiv \begin{pmatrix} \Sigma^+ & \Phi^- \\ \Phi^+ & \Sigma^- \end{pmatrix}, \tag{51}$$

where the components $\Sigma^\pm$ are the regular selfenergies and the components $\Phi^\pm$ are called gap functions. In momentum space they are the wavefunction of a diquark. The selfenergy is obtained via

$$\Sigma(p) = -\int \frac{d^4q}{(2\pi)^4} \Gamma^\mu_{0\,a} \mathcal{S}(q) \Gamma^\nu_b(p,q) D^{\mu\nu}_{ab}(p-q). \tag{52}$$

Again we encounter a feature of DSEs that a 2-point function is related to other 2- and 3-point functions. Only this time we have to deal with an additional 2×2 matrix structure in Nambu-Gor'kov space.
In order to get the full quark propagator we have to solve the Dyson-Schwinger equations, Eq.(48), self-consistently. In Nambu-Gor'kov space we denote the full quark propagator by

$$\mathcal{S} = \begin{pmatrix} S^+ & T^- \\ T^+ & S^- \end{pmatrix} \tag{53}$$

where $T^\pm$ are called the anomalous propagators that are characteristic for colour superconductivity.

We can compute the components of $\mathcal{S}$ by formally inverting its Nambu-Gor'kov structure and using the DSE, Eq. (48). The resulting matrix equation can then be solved for its components. We end up with the following set of equations

$$T^{\pm} = -Z_{1F}\left(Z_2 S_0^{\mp -1} + Z_{1F}\Sigma^{\mp}\right)^{-1}\Phi^{\pm}S^{\pm}, \tag{54}$$

$$S^{\pm -1} = Z_2 S_0^{\pm -1} + Z_{1F}\Sigma^{\pm} - Z_{1F}^2\Phi^{\mp}\left(Z_2 S_0^{\mp -1} + Z_{1F}\Sigma^{\mp}\right)^{-1}\Phi^{\pm}, \tag{55}$$

for the normal and anomalous quark propagator. Eq. (55) is identical to the QCD gap equation Eq. (25), except that it is now coupled to the gap functions. If the gap function vanishes, i.e. we have a non-superconducting state, Eq. (55) reduces to the familiar QCD gap equation, as we expect it.
The connection to the order parameter of colour superconductivity, the diquark condensate, Eq. (40), can be established using

$$\left\langle \psi^T C\mathcal{O}\psi \right\rangle = -Z_{1F}Z_2 \int \frac{d^4p}{(2\pi)^4}\ \mathrm{Tr}\left[C\mathcal{O}T^{+}\right] \tag{56}$$

The gap functions are not the energy gaps in the excitation spectrum of the quasiparticles. However they are closely related to the gaps in the excitation spectrum and will be used to estimate the size of the gap.
To compute the normal selfenergy and the gap functions we have to know the quark-gluon vertex and the gluon propagator. The bare and full vertex in Nambu-Gor'kov space are given by

$$\Gamma^{\mu}_{0\,a} = \begin{pmatrix} \frac{i}{2}g\gamma^{\mu}\lambda_a & 0 \\ 0 & -\frac{i}{2}g\gamma^{\mu}\lambda_a^T \end{pmatrix}, \quad \Gamma^{\mu}_{a}(p,q) = \begin{pmatrix} ig\Gamma_a^{+,\mu}(p,q) & X_a^{-,\mu}(p,q) \\ X_a^{+,\mu}(p,q) & -ig\Gamma_a^{-,\mu}(p,q) \end{pmatrix}. \tag{57}$$

The quark-gluon vertex satisfies its own DSE, that we will not solve. Instead we will approximate the vertex. The first approximation is that the vertex is diagonal in Nambu-Gor'kov space: $X^{\pm} = 0$. This means neglecting off-diagonal elements that could be induced in a colour-superconducting state. This must be subject of further investigations because it is not clear why there should not be off-diagonal elements. However, their influence on the results is presumably small, since we expect them to be induced.
Furthermore we employ the abelian approximation already used in the non-superconducting phase. The 11-component in Nambu-Gor'kov space of the quark-gluon vertex is:

$$\Gamma_a^{+,\mu}(p,q) = \Gamma((p-q)^2)\gamma^{\mu}\frac{\lambda_a}{2}, \tag{58}$$

where $\Gamma(k^2)$ is taken from quenched vacuum studies. We will specify the 22-component later.
The gluon propagator does not undergo any changes compared to the non-superconducting phase, because we only modified the fermionic part of the theory. Thus the gluon propa-

gator is given by Eq. (39). The selfenergies are

$$\Sigma^+ = -4\pi\frac{Z_2}{Z_{1F}}\int\frac{d^4q}{(2\pi)^4}\,\gamma^\mu\frac{\lambda_a}{2}S^+(q)\gamma^\nu\frac{\lambda_a}{2}\left(\frac{\alpha(k^2)}{k^2+G(k)}P^T_{\mu\nu}+\frac{\alpha(k^2)}{k^2+F(k)}P^L_{\mu\nu}\right) \quad (59)$$

$$\Sigma^- = -4\pi\frac{Z_2}{Z_{1F}}\int\frac{d^4q}{(2\pi)^4}\,\gamma^\mu\frac{\lambda_a^T}{2}S^-(q)\gamma^\nu\frac{\lambda_a^T}{2}\left(\frac{\alpha(k^2)}{k^2+G(k)}P^T_{\mu\nu}+\frac{\alpha(k^2)}{k^2+F(k)}P^L_{\mu\nu}\right) \quad (60)$$

$$\Phi^+ = 4\pi\frac{Z_2}{Z_{1F}}\int\frac{d^4q}{(2\pi)^4}\,\gamma^\mu\frac{\lambda_a^T}{2}T^+(q)\gamma^\nu\frac{\lambda_a}{2}\left(\frac{\alpha(k^2)}{k^2+G(k)}P^T_{\mu\nu}+\frac{\alpha(k^2)}{k^2+F(k)}P^L_{\mu\nu}\right) \quad (61)$$

$$\Phi^- = 4\pi\frac{Z_2}{Z_{1F}}\int\frac{d^4q}{(2\pi)^4}\,\gamma^\mu\frac{\lambda_a}{2}T^-(q)\gamma^\nu\frac{\lambda_a^T}{2}\left(\frac{\alpha(k^2)}{k^2+G(k)}P^T_{\mu\nu}+\frac{\alpha(k^2)}{k^2+F(k)}P^L_{\mu\nu}\right), \quad (62)$$

where $k = p - q$ and the projectors P^T and P^L are defined relative to k.
To reduce the number of variables being used, we can use the fact that the components of the quark propagator in Nambu-Gor'kov space are related to each other due to the constraint that the action must be real and invariant under charge conjugation [3, 27]. These relations are:

$$S^-(p) = -C(S^+(-p))^T C \quad (63)$$

$$T^-(p) = \gamma_4(T^+(p))^\dagger\gamma_4 \quad (64)$$

where $C = \gamma_2\gamma_4$ is the charge conjugation matrix introduced above. We also have relations for the quark-gluon-vertex:

$$\Gamma^{-,\mu}_a(p,q) = -C(\Gamma^{+,\mu}_a(-p,-q))^T C$$

$$X^{-,\mu}_a(p,q) = \gamma_4(X^{+,\mu}_a(p,q))^T\gamma_4$$

and for the selfenergy:

$$\Sigma^-(p) = -C(\Sigma^+(-p))^T C \quad (65)$$

$$\Phi^-(p) = \gamma_4(\Phi^+(p))^\dagger\gamma_4 \quad (66)$$

this allows us to use only the "+" components of the quark propagator in Nambu-Gor'kov space.

2.5 Colour-Spin locking

Symmetries in one-flavour colour superconductors

In perturbative QCD one-gluon exchange is the dominating interaction between quarks. It is attractive in the antisymmetric colour antitriplet channel, therefore, we will focus on pairing in this channel.
For relativistic particles, spin S and angular momentum L are not themselves good quantum numbers, the total spin $J = L + S$ is a good quantum number. This is why possible diquark wave functions should be classified by their total spin J. In the antisymmetric colour triplet channel, a single quark flavour cannot pair in the total spin $J = 0$ channel,

but in the $J = 1$ channel. This owes to the fact that the wavefunction must be antisymmetric. An exhaustive discussion of possible pairing patterns for a single quark flavour can be found in [16, 28]. The diquark wavefunction can also contain contributions of total spin different from $J = 1$, these contributions are in the symmetric colour channel and are induced by the pairing in the $J = 1$ channel.
For the pairing of quarks to total spin $J = 1$ in an antisymmetric colour channel, the operator $\mathcal{O}$ in Eq. (40) therefore needs to be build up by the generators of $SO(3)_c$ and $SU(2)_J$. $SO(3)_c \subset SU(3)_c$ is the rotational subgroup of $SU(3)_c$, its generators are the generators of rotations. However, they act in colour space. We will associate $SO(3)_c$ with a 'colour spin' Ω. $SU(2)_J$ is the group of rotations acting in real space, it is locally isomorphic to $SO(3)_J$.
The precise pairing pattern is determined by the coupling of $SO(3)_c$ and $SO(3)_J$. The so called colour spin locked phase is defined by locking total spin $\vec{J}$ and colour spin $\vec{\Omega}$, such that $SO(3)_c \times SO(3)_J$ is broken down to $SO(3)_{c+J}$. Another spin-1 phase is the polar phase, that locks only the 3-components of colour and total spin.
As discussed in section 2.4, the starting point for the investigation of a colour-superconducting phase is the order parameter, the diquark condensate. The operator $\mathcal{O}$ in Eq. (40) is build up by the generators of $SO(3)_c$ and $SU(2)_J$. Thus a general parametrisation of the diquark condensate, Eq. (40), in a spin-1 phase is of the form

$$\Delta_{ij}\langle\bar{\psi}_c\lambda_i\gamma_j\psi\rangle \tag{67}$$

where the gamma matrices $\gamma_1, \gamma_2, \gamma_3$ are the spatial generators of $SU(2)_J$ and the λ_i's are the antisymmetric generators of $SO(3)_c$, i.e. $\vec{\lambda} = (\lambda_7, -\lambda_5, \lambda_2)$. The 3×3 matrix Δ parametrises the order parameter that spontaneously breaks the original symmetry group of the system. In the present case this symmetry group is $SO(3)_c \times SO(3)_J$. The transformation behaviour of Δ in Eq. (67) is then given by

$$\Delta \to \Delta' = U^T \Delta V, \tag{68}$$

where $U \in SO(3)_c$ and $V \in SO(3)_J$.

CSL symmetry

The colour-superconducting phase we are going to consider throughout the rest of this work is the so called colour-spin locked (CSL) phase . It is a spin-1 phase, that turned out to be the most stable spin-1 colour-superconducting phase in the weak coupling regime [16]. It is characterised by the locking of total spin $\vec{J}$ and 'colour spin' $\vec{\Omega}$. The CSL phase is symmetric under a joint transformation of $\vec{J}$ and $\vec{\Omega}$ that we will call CSL transformation. The CSL phase is given by setting (cf. [16])

$$\Delta = \begin{pmatrix} 1 & 0 & 0 \\ 0 & 1 & 0 \\ 0 & 0 & 1 \end{pmatrix}. \tag{69}$$

Remember that the transformation behaviour of Δ in Eq. (67) is given by

$$\Delta \to \Delta' = U^T \Delta V, \tag{70}$$

where $U \in SO(3)_c$ and $V \in SO(3)_J$. It is immediately clear that the condensate is invariant under a CSL transformation, if $U^T = V^{-1}$. Since U and V are orthogonal matrices this implies $U^T = V^{-1} = V^T$. This clarifies the name "colour-spin locking".
We will now elaborate on the CSL symmetry in order to derive the most general ansatz for a CSL symmetric phase. One flavour QCD exhibits $SU(3)_c \times SO(3)_J \times U_A(1)$ symmetry. In the presence of a diquark condensate this symmetry will be broken. As explained above, in the colour-spin locked phase $SO(3)_c$ and $SO(3)_J$ are, in the presence of the diquark condensates, broken down to a $SO(3)_{c+J}$ symmetry. We saw that only a combination of $SO(3)_c$ and $SO(3)_J$ preserves CSL symmetry. $\frac{1}{2}\vec{\sigma} + \vec{L}$ are the generators of $SO(3)_J$, where $\vec{\sigma} = i\gamma_5\gamma_4\vec{\gamma}$ and $\vec{L}$ are the angular momentum operators. $\vec{\lambda} = (\lambda_7, -\lambda_5, \lambda_2)$ are the generators of $SO(3)_c$ and also antisymmetric generators of $SU(3)_c$. The generators of a CSL transformation are:

$$\vec{G} \;=\; \frac{1}{2}\vec{\sigma} + \vec{L} + \vec{\lambda}. \tag{71}$$

One can verify that the generators $\vec{G}$ satisfy the $SO(3)$ commutation relations

$$[G_i, G_j] = i\epsilon_{ijk}G_k. \tag{72}$$

Confirming that the breaking pattern

$$SU(3)_c^a \otimes SO(3)_J \to SO(3)_{c+J} \tag{73}$$

is realized.

The CSL ansatz

Having defined the CSL phase and determined its symmetry pattern, we can elaborate on the most general parametrisation of the propagator S^+, the anomalous propagator T^+, the normal selfenergy Σ^+ and the gap function Φ^+.
Therefore we have to find all tensor structures P_a that are invariant under a CSL transformation, i.e $P_a = P'_a = U^\dagger P_a U, \quad U \in SO(3)_{c+J}$. These are

$$\begin{aligned}
P_{1,ij} &= \gamma_4\delta_{ij} \\
P_{2,ij} &= \gamma_5\gamma_4 \left(\hat{p}\cdot\vec{\lambda}_{ij}\right) \\
P_{3,ij} &= i\gamma_5 \left(\vec{\gamma}\cdot\vec{\lambda}_{ij}\right) \\
P_{4,ij} &= \gamma_4 \left(\hat{p}_i\hat{p}_j\right) \\
P_{5,ij} &= \left(\gamma_i\hat{p}_j + \hat{p}_i\gamma_j\right) \\
&\gamma_5 \quad , \quad \not{\hat{p}}
\end{aligned}$$

and scalars in colour-spin space. The notation is such that Dirac indices are supressed and i, j are colour indices. An example is instructive, α, β are Dirac indices:

$$(P_3)_{ij}^{\alpha\beta} = \sum_{a=1}^{3} (\lambda_a)_{ij}\ (\gamma_5\gamma_a)^{\alpha\beta}.$$

These tensor structures form an algebra, thus we can be assured that an ansatz containing all tensor structures is selfconsistent. The full ansatz for the an even parity gap function is

$$\Phi^+ = \sum_{i=1}^{5} \left(\phi_{C,i} + i\gamma_4 \hat{\not{p}} \phi_{A,i} + \gamma_4 \phi_{B,i} + i\hat{\not{p}} \phi_{D,i}\right) \ \gamma_5 \ P_i. \tag{74}$$

Remember that $\not{p} = \hat{p} \cdot \vec{\gamma}$.
One also has to make sure that a colour-superconducting phase does not carry a colour charge. The colour charge is proportional to

$$\rho^a(x) \propto \frac{1}{2} \mathrm{Tr}_{D,c,NG} \left[\mathcal{S}(x) \Gamma_4^{(0)a}\right]. \tag{75}$$

We checked that in our ansatz after performing the traces and integrating the colour charge vanishes.

Coupled channels

The general idea behind this ansatz is to couple the abstract spins, the diquark carries, to zero total spin. These spins are the total spin of the quark-antiquark pair, given by its spin and its angular momentum, and their 'colour spin'.
The colour structure of a single quark spinor transforms under a CSL transformation in the adjoint representation, i.e. like a spin 1 particle. Two quarks can therefore couple to 'colour spin' 0, 1 and 2. In 3×3 matrix representation of the group $SO(3)_c$, this corresponds to unity, antisymmetric and symmetric matrices respectively.
The spins can couple to spin 0 and 1, which is given by a unit matrix in Dirac space and $\vec{\sigma} = i\gamma_5\gamma_4\vec{\gamma}$, respectively.
Finally the orbital angular momenta have to couple the sum of colour and spin transformation exactly to zero in order to get a invariant expression for the propagator. Therefore, we will need $L = 0, 1, 2, 3$ contributions to the gap function.
This now allows us to determine the number of tensor structures needed to construct the full ansatz. Therefore, we count the number of different ways of coupling spin (S=0,1) and 'colour spin' (ω=0,1,2). For S=0 we can couple ω and S in three different ways to 0,1 and 2. We can couple S=1 with ω=0 in one way to 1, with ω=1 in three ways to 0,1,2 and with ω=2 in three ways to 1,2,3. So we have alltogether 10 different ways of coupling ω and S. This number doubles for massive quarks because in this case we have two distinct quark doublets of opposite chirality.

3 Colour-Spin locking with an ansatz for the colour-spin structure

A first approach to the colour-spin locked phase is to constrain the ansatz for the gap function, Eq. (74), in a manner that allows, to some extend, treating the problem analytically. Therefore, we will concentrate on the attractive channels and fix the colour structure of the gap function. This ansatz for the gap function is not self-consistent and needs to be investigated further. Still it is a good exercise to gain first insight into the properties of the colour-spin locked phase.
Having defined the ansatz for the gap function, the next step will be to compute the quark propagator and the anomalous propagator, eventually we will arrive at the gap equation and solve it numerically.

3.1 Ansatz for the colour-spin structure of the gap function

We start with an Ansatz for the structure of the gap function as proposed e.g. in [16, 29]. The quarks under consideration are assumed to be massless. Then we parametrise the gap function by

$$\Phi^+(p) \;=\; \frac{Z_2}{Z_{1F}} \sum_{e=\pm} \phi_e(p) \Lambda^e_{\hat{p}} \mathcal{M}_{\hat{p}}, \tag{76}$$

where we introduced energy projectors and the scalar gap function ϕ_e:

$$\Lambda^{\pm}_{\hat{p}} = \frac{1}{2}\left(1 \pm i \frac{\gamma_4 \vec{p}\vec{\gamma}}{|\vec{p}|}\right). \tag{77}$$

The use of energy projectors allows for a good interpretation of the results, because the coefficient functions to the energy projectors are related to the energy gaps in the excitation spectrum. This will become clear when we have an expression for the quark propagator.
The matrix $\mathcal{M}_{\hat{p}}$ defines the colour, flavour and (partly) Dirac structure of the gap function. It is implicitly defined by the CSL symmetry of the colour-superconducting phase since it is a part of Φ^+. We also have the freedom to chose it such that it commutes with the energy projectors $\Lambda^{\pm}_{\hat{p}}$:

$$\left[\mathcal{M}_{\hat{p}}, \Lambda^{\pm}_{\hat{p}}\right] = 0. \tag{78}$$

This is achieved by setting [27]

$$\mathcal{M}_p = \vec{\lambda} \cdot \left(\alpha \hat{p} + \beta i \vec{\gamma}_\perp(\hat{p})\right), \tag{79}$$

where we defined $\vec{\gamma}_\perp(\hat{p}) \equiv \vec{\gamma} - \hat{p}(\hat{p}\cdot\vec{\gamma})$. The antisymmetric 3x3 matrices $(\lambda_i)_{jk} = -i\epsilon_{ijk}$, $i,j,k = 1,2,3$ form a basis of the colour antitriplet. At this point it can be seen that we are considering the attractive channel of the diquark wave function. α and β are freely adjustable parameters for which we require $\alpha^2 + \beta^2 = 1$. Since rescaling of α

and β does not change any observable (cf. [16]), this can safely be done.
In Eq. (79) the first term on the right hand side, proportional to $\hat{p}_i$, describes pairing of quarks with the same chirality. This is easily understood since it commutes with the chirality projectors $(1 \pm \gamma_5)/2$. By contrast the second term, proportional to $\vec{\gamma}_\perp(\hat{p})$ corresponds to pairing of quarks of opposite chirality. Again this can be seen by commuting it with the chirality projectors and noting that it flips the sign of chirality.
As in [16], we will consider only two of the infinitely many possible parametrisations of the gap function

- $\alpha = 0\ ,\ \beta = 1$ called the "transverse case"
- $\alpha = \beta = \frac{1}{\sqrt{2}}$ called the "mixed case"

This nomenclature was introduced in [16, 30]. The choice $\mathcal{M}_p = i\vec{\lambda} \cdot \vec{\gamma}_\perp(\hat{p})$ uses a Dirac structure that is perpendicular to $\vec{p}$ in real space, that justifies the name "transverse case". Since the choice $\alpha = \beta$ implies an admixture of $\vec{\lambda} \cdot \hat{p}$, that has been called "longitudinal" in [30], it is reasonable to call this choice "mixed case".
With Eq. (76) we compute an identity, which will be important for obtaining the full quark propagator,

$$\Phi^- \left(Z_2[S_0^-]^{-1} + Z_{1F}\Sigma^-\right)^{-1} \Phi^+ \left(Z_2[S_0^-]^{-1} + Z_{1F}\Sigma^-\right) = \left(\frac{Z_2}{Z_{1F}}\right)^2 \sum_{e=\pm} |\phi_e|^2 \, L_{\hat{p}} \Lambda_{\hat{p}}^{-e}, \tag{80}$$

where we defined $L_{\hat{p}} = \gamma_4 \ \mathcal{M}_{\hat{p}}^\dagger \ \mathcal{M}_{\hat{p}} \ \gamma_4$. The commutation properties of the matrix $\mathcal{M}_{\hat{p}}$ are important for deriving this result. Using the parametrisation of the gap matrix, Eq. (79), we can write the matrix $L_{\hat{p}}$ explicitely:

$$(L_{\hat{p}})^{mn} = (\alpha^2 + 2\beta^2)\delta^{mn} - \left[\alpha\hat{p}^m + \beta i\gamma_\perp^m(\hat{p})\right]\left[\alpha\hat{p}^n - \beta i\gamma_\perp^n(\hat{p})\right], \tag{81}$$

where m, n are colour indices and we supressed Dirac indices. The eigenvalues of the matrix $L_{\hat{p}}$ are

$$\lambda_{1,2} = \tfrac{1}{2}\alpha^2 + 2\beta^2 \pm \alpha\sqrt{\alpha^2 + 8\beta^2} \quad \text{(4-fold each)} \quad \lambda_3 = \alpha^2 \quad \text{(4-fold)}. \tag{82}$$

Since $L_{\hat{p}}$ is a hermitian matrix, it has real eigenvalues λ_r and can be expanded in terms of a complete set of orthogonal projectors, $\mathcal{P}_{\hat{p}}^r$. With our parametrisation of $\mathcal{M}_{\hat{p}}$ we can see from Eq. (82) that there are only two distinct eigenvalues for the cases under consideration. The projectors can be obtained using the formula

$$\mathcal{P}_{\hat{p}}^{1/2} = \frac{L_{\hat{p}} - \lambda_{2/1}}{\lambda_{1/2} - \lambda_{2/1}}. \tag{83}$$

Since the matrix $\mathcal{M}_p$ commutes with the energy projectors so does the matrix $L_{\hat{p}}$ and consequently also the projectors onto eigenspaces of $L_{\hat{p}}$, $\mathcal{P}_{\hat{p}}^r$: $\left[\mathcal{M}_{\hat{p}}, \mathcal{P}_{\hat{p}}^r\right] = 0$. This property will be used extensively in the following.

3.2 The quark propagator and the gap equation

Using the results above we can now compute the inverse full propagator, this is done in appendix C. First, however, we have to introduce a notation for the normal quark selfenergy. Since the quark propagator will be decomposed onto energy projectors and the projectors $\mathcal{P}^r_{\hat{p}}$, it would be reasonable to do the same decomposition with the normal quark selfenergy. It would presumably be given by

$$\Sigma^+(p) = \frac{Z_2}{Z_{1F}} \sum_{e=\pm,r} \left(e|\vec{p}|\Sigma_{A,r}(p) + i\omega_p \Sigma_{C,r}(p)\right) \ \gamma_4 \mathcal{P}^r_{\hat{p}} \Lambda^e_{\hat{p}}. \tag{84}$$

However, the inverse full quark propagator, Eq. (55), can then not be inverted analytically. Therefore, we make the assumption, that in Eq. (84) $\Sigma_{A,1} \equiv \Sigma_{A,2} \equiv \Sigma_A$ and likewise $\Sigma_{C,1} \equiv \Sigma_{C,2} \equiv \Sigma_C$. Since the sum $\mathcal{P}^1_{\hat{p}} + \mathcal{P}^2_{\hat{p}}$ is the identity matrix in colour and Dirac space, the normal quark selfenergy is given by

$$\Sigma^+(p) = \frac{Z_2}{Z_{1F}} \sum_{e=\pm,r} \left(e|\vec{p}|\Sigma_A(p) + i\omega_p \Sigma_C(p)\right) \ \gamma_4 \Lambda^e_{\hat{p}}. \tag{85}$$

The normal quark selfenergy Σ^+ is computed using Eq. (59). Since we expect the gaps to be rather small, we approximate the full quark propagator in Eq. (59) by the full quark propagator that we obtain by solving Eq. (24), i.e. for quark matter in the non-superconducting state.
Doing this approximation is not a neglect, but dictated by the CSL phase. Yet the implications are not too serious since we will include the normal selfenergy self-consistently in the next section, where we will also treat the gap function self-consistently.
The full propagator is

$$S^+(p) \ = \ \frac{1}{Z_2^2} \sum_{e=\pm,r} \frac{-e|\vec{p}|(1+\Sigma^*_A(p)) + i\omega^*_p(1+\Sigma^*_C(p))}{\left|e|\vec{p}|(1+\Sigma_A(p)) + i\omega_p(1+\Sigma_C(p))\right|^2 + \lambda_r \left|\phi_e(p)\right|^2} \gamma_4 \mathcal{P}^r_{\hat{p}} \Lambda^{-e}_{\hat{p}}. \tag{86}$$

This results allows for an illuminating interpretation. The poles of the full propagator that define the excitation spectrum are given by the solution of the equation

$$\begin{aligned} 0 \ &= \ \left|e|\vec{p}|(1+\Sigma_A(p)) + i\omega_p(1+\Sigma_C(p))\right|^2 + \lambda_r \left|\phi_e(p)\right|^2 \\ &= \ \left|e|\vec{p}|(1+\Sigma_A(p)) + i(p4+i\mu)(1+\Sigma_C(p))\right|^2 + \lambda_r \left|\phi_e(p)\right|^2. \end{aligned} \tag{87}$$

For conciseness let us neglect the normal quark selfenergies Σ_A and Σ_C and approximate the gap functions $\phi_e(p)$ by a real constant, Δ. This will affect the dispersion excitation spectrum only quantitatively. Then the poles are located where $p_4^2 + (e|\vec{p}| - \mu)^2 + \lambda_r \Delta^2 = 0$. Finally we establish the connection with Minkowski space by the relation $p_4^2 = -p_0^2$, where p_0 is the zero component of the momentum in Minkowski space. The poles are now located at

$$p_0 = \pm\sqrt{(e|\vec{p}| - \mu)^2 + \lambda_r \Delta^2}. \tag{88}$$

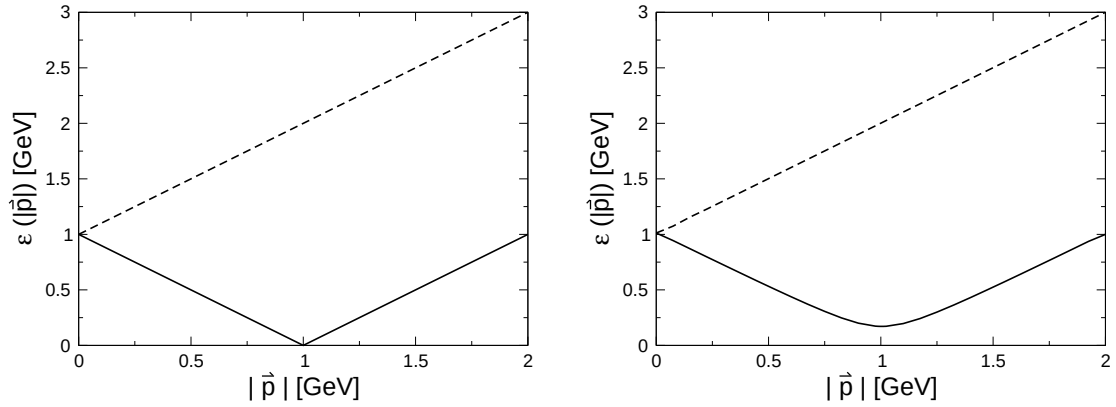

Figure 7: The excitation spectrum for quasiparticles in a non-superconducting state (left) and in a superconductor (right). The dashed lines show the quasi-antiparticles free energy ϵ, the full lines show the quasi-particles free energy.

For quasi-antiparticles and quasi-antiparticles-holes in the superconducting state, i.e. $e = -1$, the dispersion branches are almost unchanged compared to the dispersion branches for quasi-antiparticles and quasi-antiparticles-holes in the non-superconducting state. Since Δ will be very small compared to μ, $\Delta \ll \mu$, the dispersion relations are simply $p_0 \approx \pm(|\vec{p}| + \mu)$.
The dispersion branches for quasi-particles and quasi-holes, i.e. $e = +1$, in the superconducting state, however, differ significantly from the corresponding dispersion branches in the non-superconducting state. The most prominent feature is the energy gap at the Fermi surface, $|\vec{p}| = \mu$, between the quasi-particle and quasi-hole branches. Fig. 7 demonstrates the difference between the non-superconducting and the superconducting phase. The gap in the superconducting phase is artificially magnified by a factor of 30. We see that the costs in free energy to excite quasiparticle-quasihole pairs at the Fermi surface is $2\lambda_r\Delta$. Only if $\lambda_r = 0$ there is a gapless mode in the excitation spectrum.
We will comment more on the excitation spectra later, especially on the question whether there is an ungapped mode or not. For now we continue with the solution of the gap equation. The next ingredient needed to solve the DSE, is the anomalous propagator. To compute the anomalous propagator we use the identity

$$\left[Z_2(S_0^-)^{-1} + Z_{1F}\Sigma^-\right]^{-1} \Phi^+ \left[Z_2(S_0^-)^{-1} + Z_{1F}\Sigma^-\right] = \frac{Z_2}{Z_{1F}} \sum_{e'} \left[\phi_{e'}(p)\right] \gamma_4 \mathcal{M}_{\hat{p}} \gamma_4 \Lambda_{\hat{p}}^{-e'}, \quad (89)$$

that is derived in the appendix C. Using this identity, Eq. (86) and Eq. (55), the anomalous propagator can be expressed as

$$T^+(p) = \frac{1}{Z_2} \sum_{e'=\pm,r} \phi_{e'}(p) \frac{\gamma_4 \mathcal{M}_{\hat{p}} \gamma_4 \mathcal{P}^r_{\hat{p}} \Lambda^{-e'}_{\hat{p}}}{|e'|\vec{p}|(1+\Sigma_A(p)) + i\omega_p(1+\Sigma_C(p))|^2 + \lambda_r |\phi_{e'}(p)|^2} \quad (90)$$
$$=: \sum_{e'=\pm,r} \gamma_4 \mathcal{M}_{\hat{p}} \gamma_4 \mathcal{P}^r_{\vec{p}} \Lambda^{-e'}_{\hat{p}} T^+_{e',r}(p).$$

Now we can formulate the gap equation, Eq. (61), in terms of the functions ϕ_e. To get scalar equations for the functions ϕ_e we plug Eq. (90) into Eq. (61), multiply the resulting equation from the right with $\mathcal{M}^\dagger_{\hat{p}}\Lambda^e_{\hat{p}}$ and take the trace over Dirac and colour space. The resulting equations are:

$$\phi_e(p) = 4\pi \int \frac{d^4q}{(2\pi)^4} \sum_{e'=\pm,r} T^+_{e',r}(q)\mathcal{T}_r^{\mu\nu,ee'}(p,q)\left(\frac{\alpha(k^2)}{k^2+G(k)}P^T_{\mu\nu} + \frac{\alpha(k^2)}{k^2+F(k)}P^L_{\mu\nu}\right) \quad (91)$$

$$\mathcal{T}_r^{\mu\nu,ee'}(p,q) = -\frac{\mathrm{Tr}[\gamma^\mu \frac{\lambda_a}{2}\gamma^4 \mathcal{M}_{\hat{q}}\gamma^4 \mathcal{P}^r_{\hat{q}}\Lambda^{-e'}_{\hat{q}}\frac{\lambda_a}{2}\gamma^\nu \mathcal{M}^\dagger_{\hat{p}}\Lambda^e_{\hat{p}}]}{\mathrm{Tr}[\mathcal{M}_{\hat{p}}\mathcal{M}^\dagger_{\hat{p}}\Lambda^e_{\hat{p}}]} \quad (92)$$

The traces and the summation over spacetime indices are done using the program Mathematica. Integrating the resulting formulae is done numerically. A very similar procedure was used to compute the components Σ_A and Σ_C of the normal quark selfenergy.

Solutions

We solved the DSE in four different cases: For the transverse and mixed case of the CSL phase, using two different effective strong running couplings discussed in section 2.3. Examples of the scalar gap functions $\phi_\pm$ are shown in Fig. 8 and 9 for a chemical potential of $\mu = 1$ GeV, using the effective strong running coupling α_I. The use of α_{II} instead of α_I will only slightly alter the shape and the value of the scalar gap functions. Note the sharp peak in the gap function ϕ^+ for the quasiparticles and the fact that the scalar gap function for quasiparticles is about one order of magnitude larger than the gap function for anti-quasiparticles.
The focus rests on the value of the scalar gap functions at the Fermi surface since we will use these values for an estimate of the energy gaps in the excitation spectrum. As explained above, in momentum regions away from the Fermi surface the excitation spectrum

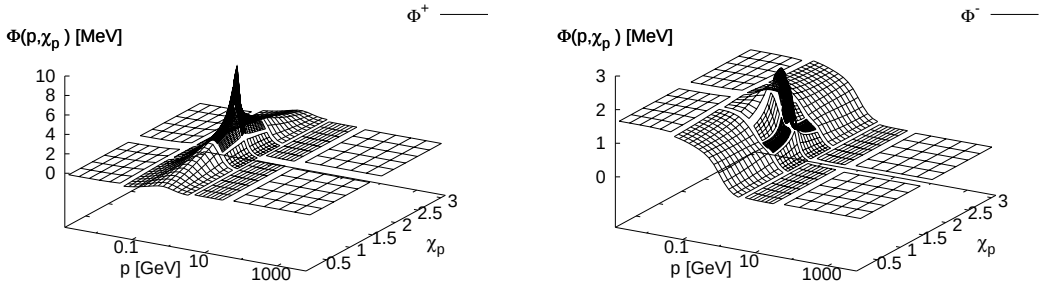

Figure 8: The gap functions $\phi^\pm(p)$ for $\mu = 1$ GeV, using the effective strong running coupling α_{II}, as a function of total momentum p and the momentum angle χ. The plots display the results for the mixed case. p is the absolute momentum, χ is in hyperspherical coordinates the angle between the spatial momentum and the temporal momentum, i.e. $p_3 = p\sin(\chi),\ p_4 = p\cos(\chi)$. A definition of these coordinates is given in appendix D.

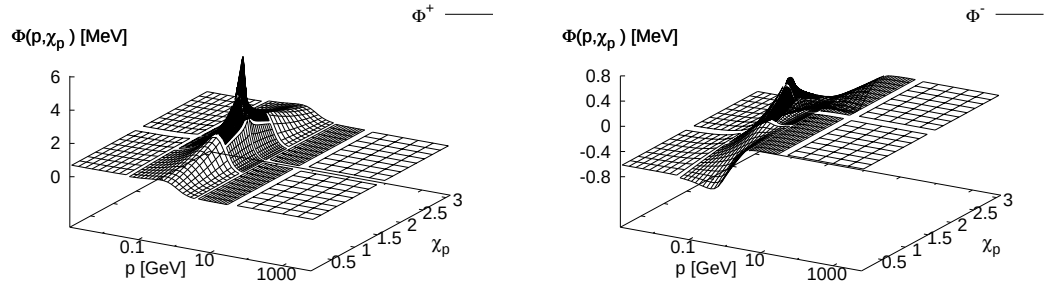

Figure 9: The gap functions $\phi^{\pm}(p)$ for $\mu = 1$ GeV, using the effective strong running coupling α_{II}, as a function of total momentum p and the momentum angle χ. The plots display the results for the transverse case.

is nearly unchanged by the presence of a diquark condensate. The behaviour of the value of the gap functions as a function of μ is shown in Fig. 10. In this figure we compared the transverse and the mixed case. We also showed the influence of the effective strong running coupling in Fig. 11.
It turns out that the influence of the choice of the effective running coupling on the gap functions is rather small. By contrast, the effect of this choice on the running quark mass is significant. Thus it is interesting to see that the size of the gaps at the Fermi surface hardly changes with the effective strong running coupling. This is encouraging because small dependence of the gap function on the effective strong running coupling affirms us that the influence of medium modifications on the gluon propagator is not going to introduce sizable effects on the gap functions.
What is surprising is the size of the scalar gap functions. Extrapolating weak coupling results [16], that are obtained for high chemical potential, to the intermediate region of

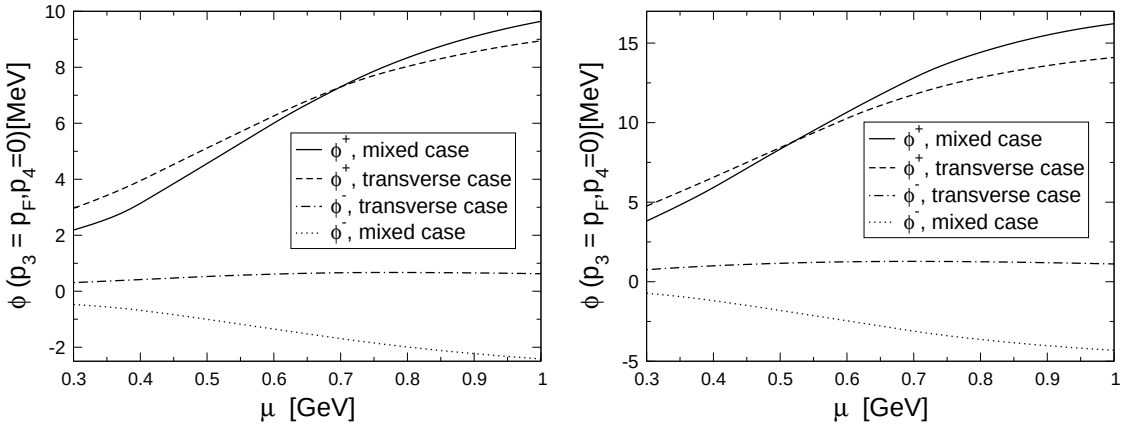

Figure 10: The peak values of the gap functions $\phi^{\pm}$ as a function of chemical potential for the two different cases. The left graph shows the results that were obtained using the effective strong running coupling α_I, in the right graph we used α_{II}.

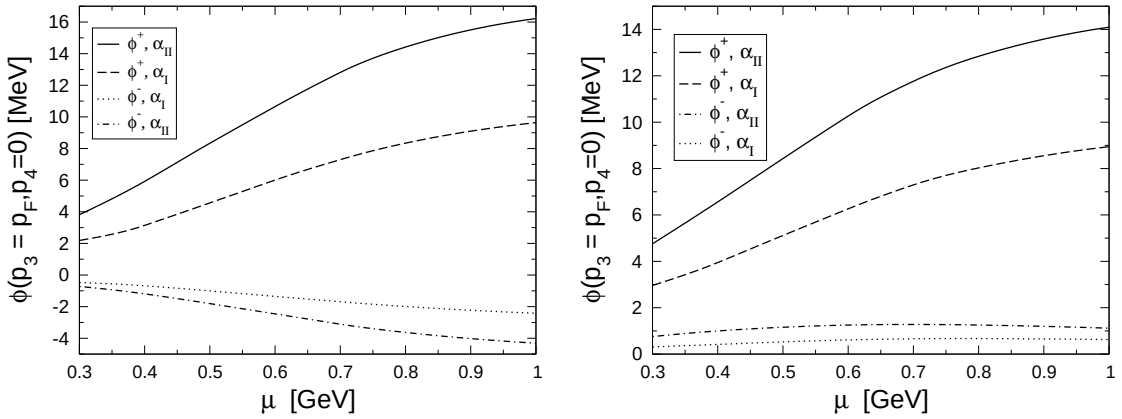

Figure 11: The peak values of the gap functions $\phi^{\pm}$ as a function of chemical potential and the influence of the strong running coupling. In the left graph the results for the mixed case are displayed, the right graph shows the results for the transverse case.

the chemical potential we are working in, one would have expected values of 100 keV - 1 MeV for the size of the scalar gap functions. That our result is about one ot two orders of magnitude larger owes to some part that an extrapolation of a weak coupling result is not reliable in this region. Previous calculations [23] showed that in the intermediate region of the chemical potential the values of the gap function at the Fermi surface is significantly larger.
Another difference to the weak coupling results is that the values of the gap function at the Fermi surface in the CSL phase are not as supressed in our calculation as it is in the weak coupling limit. There, however, the longitudinal parts of the gluon propagator lead to a larger supression that we do not observe in our calculations.

3.3 CJT pressure difference

The CSL phase is not the only possible colour-superconducting spin-1 phase. A priori it is not apparent, which of the possible phases is being realised in nature. This question can be decided by finding the phase that minimises the effective potential V_{eff}. At the stationary point of the effective potential this is equivalent to finding the maximum of the thermodynamic pressure or the maximum of the effective action $\mathcal{A}$. Thus we search for the maximum of the effective action. For our purposes it is sufficient to compute only the pressure difference between the superconducting and the non-superconducting phases.
In weak coupling studies it was found that the transverse CSL phase is the most stable spin-1 phase [16]. It will be interesting to explore whether the same holds true in our approach.
The starting point is the effective action. We neglect the backreaction of the quarks onto the gluon sector, thus the only part of the effective action that is varying between superconducting and non-superconducting phases is given by (cf. [16])

$$\mathcal{A}[\mathcal{S}] = -\frac{1}{2}\mathrm{Tr}_{p,D,c,N}[\mathrm{Ln}\mathcal{S}^{-1}] + \frac{1}{2}\mathrm{Tr}_{p,D,c,N}[1 - \mathcal{S}_0^{-1}\mathcal{S}] - \Gamma_2[\mathcal{S}]. \tag{93}$$

The functional $\Gamma_2[\mathcal{S}]$ denotes the sum of all two-particle irreducible diagrams without external legs and with internal lines given by the gluon and quark propagators. $\mathrm{Tr}_{p,D,c,N}$ denotes the trace over Nambu-Gor'kov, Dirac and colour space and the integration over momentum space.
Because we cannot solve the quark DSE exactly, we have to approximate $\Gamma_2[\mathcal{S}]$. This was done in [16] and we get:

$$\Gamma_2[\mathcal{S}] \simeq \tfrac{1}{4}\mathrm{Tr}_{p,D,c,N}[\Sigma\mathcal{S}] = \tfrac{1}{4}\mathrm{Tr}_{p,D,c,N}[1 - \mathcal{S}_0^{-1}\mathcal{S}]. \tag{94}$$

Thus we end up with

$$\mathcal{A}[\mathcal{S}] = -\tfrac{1}{2}\mathrm{Tr}_{p,D,c,N}[\mathrm{Ln}\mathcal{S}^{-1}] + \tfrac{1}{4}\mathrm{Tr}_{p,D,c,N}[1 - \mathcal{S}_0^{-1}\mathcal{S}]. \tag{95}$$

We can evaluate the traces analytically and use the results to compute the effective action. The details can be found in appendix C.
To check the results we make an estimate for the pressure difference, using the formula

$$\Delta p_{est} = \frac{\mu^2 \mathrm{Tr}[L_{\hat{p}_F}]}{16\pi^2}(\phi^+(p_F))^2, \tag{96}$$

that was derived in the weak coupling limit [16]. Here $\phi^+(p_F)$ denotes that the gap function is evaluated at the Fermi surface. This is an approximation to the effective action $\mathcal{A}[\mathcal{S}]$ and should not be taken as an exact benchmark for our results.

Results

To decide which is the preferred phase we compare the pressure difference of the mixed and the transverse phase to normal quark matter. The two cases will be compared for the two effective strong running couplings α_I and α_{II} seperately. We will concentrate on the physically interesting region from 300 MeV to 500 MeV chemical potential. The results are shown in Fig. 12. In both cases the mixed case yields a higher pressure and is thus the stable phase. This is interesting, since it is not in agreement with the weak coupling result [16]. Comparing the pressure difference calculated using Eq. (95) and the estimate for the pressure difference, Eq. (96), it turns out that the estimate is surprisingly good.

Coherence lenght

Finally we also computed the coherence length, the method is described in [31], and contrasted it with the mean particle distance $\lambda = \sqrt[3]{\pi^2}/\mu$ of non-interacting quarks as determined from the density. The results is shown in Fig. 13 as a function of chemical potential μ. The results are larger than for spin-0 phases [23], however, not substantially larger. This can be understood with the behaviour of the Pippard length $\xi_P = 1/\pi\phi_+(p_F)$, which gives a rough estimate of the coherence length. Since the scalar gap function $\phi_+(p_F)$ in the CSL phase is not substantially smaller than in the spin-0 phases, the coherence length is not substantially larger. Furthermore is the density larger and therefore the ration ξ/λ is smaller.

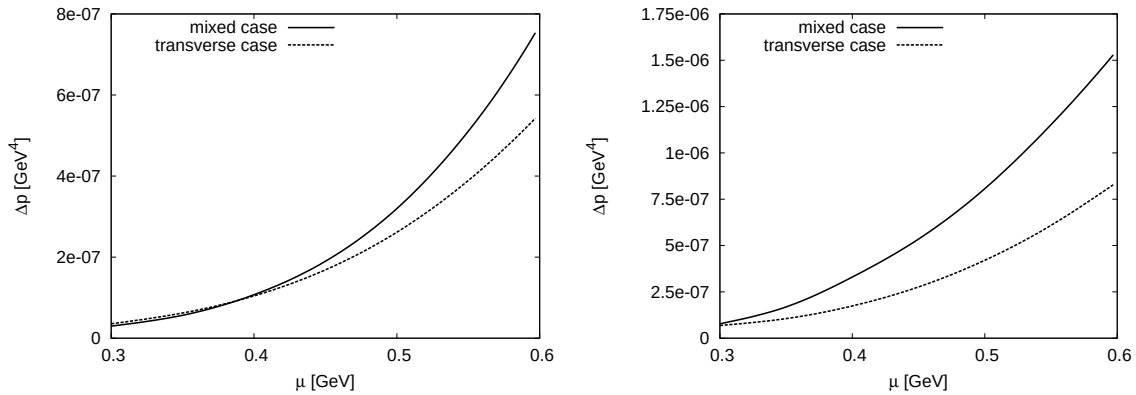

Figure 12: The pressure difference between superconducting and non-superconducting quark matter as a function of chemical potential comparing the mixed and the transverse case. The left graph shows the results that were obtainded using the effective strong running coupling α_I, in the right graph we used α_{II}.

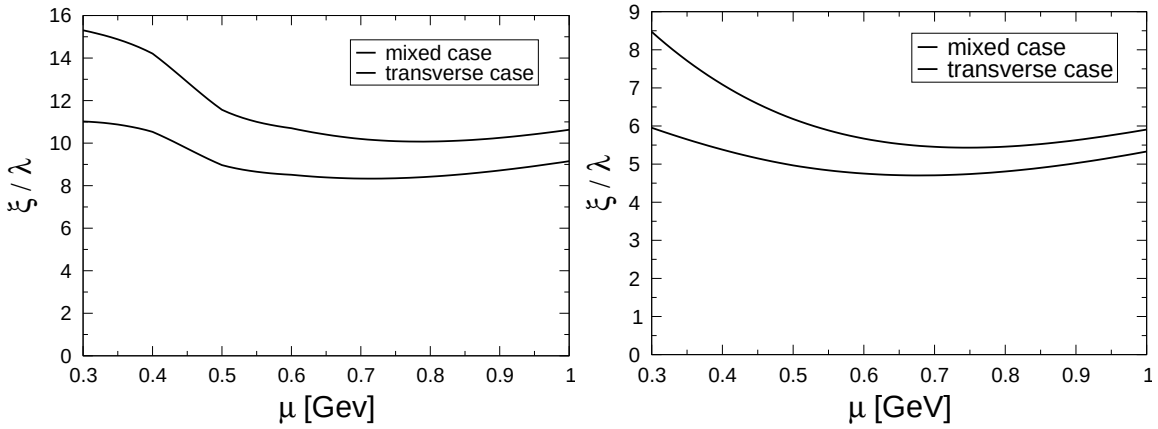

Figure 13: The coherence ξ divided by the mean free path λ. The left graph shows the results that were obtainded using the effective strong running coupling α_I, in the right graph we used α_{II}.

4 Colour-spin locking with self-consistent colour-spin structure

Until now we only considered a fixed colour-spin structure of the gap matrix. Since this truncation is not self-consistent, this is unsatisfactory. Thus we aim for a selfconsistent, dynamic determination of the gap structure in the CSL phase. We already determined the maximally allowed set of colour-spin tensor structures that is invariant unter a CSL-transformation in section 2.5. In this section we are first going to consider massless quarks, this allows us to impose chirality and furthermore parity conditions, which reduce the number of colour-spin tensor structures needed for a selfconsistent solution. Later we will extend the analysis to massive quarks which has important implications on the excitation spectrum.

4.1 QCD symmetries

We will briefly discuss some symmetries of QCD that allow us to simplify the calculation and especially reduce the numerical effort.

Parity

Parity is a discrete symmetry, it sends $(t, \vec{x}) \to (t, -\vec{x})$. In momentum space this means that a three momentum vector is sent to its negative: $\vec{p} \to -\vec{p}$. A Dirac spinor in coordinate space transforms under parity like $\psi'(t, \vec{x}) = \eta_P \gamma_4 \psi(t, -\vec{x})$, where $\eta_P = \pm 1$ is the intrinsic parity. Using this result we can determine how charge conjugate spinors transform under a parity transformation $\bar{\psi}'_C(t, \vec{x}) = -\bar{\psi}_C(t, -\vec{x})\gamma_4 \eta_P$. Using these two results we know that the Nambu-Gor'kov propagator transforms under parity as

$$\mathcal{S}'(\vec{p}) = \begin{pmatrix} \gamma_4 & 0 \\ 0 & -\gamma_4 \end{pmatrix} \mathcal{S}(-\vec{p}) \begin{pmatrix} \gamma_4 & 0 \\ 0 & -\gamma_4 \end{pmatrix}, \tag{97}$$

in components: $S'(\vec{p}) = \gamma_4 S(-\vec{p})\gamma_4$ and $T'(\vec{p}) = -\gamma_4 T(-\vec{p})\gamma_4$. In this chapter we will only consider the '+'-components of the Nambu-Gorkov space since we can always translate the '-'-components into '+'-components by virtue of the Eqns. (63) - (65). We say, that the phase has even parity, if $S'(p) = S(p)$ and $T'(p) = T(p)$. Odd parity is defined by $S'(p) = S(p)$ and $T'(p) = -T(p)$. Written explicitly, we require for an even/odd parity phase:

$$S(\vec{p}) = \gamma_4 S(-\vec{p})\gamma_4, \tag{98}$$

$$T(\vec{p}) = \mp \gamma_4 T(-\vec{p})\gamma_4 \tag{99}$$

Chirality

A chiral transformation is a symmetry of the kinetic term in the QCD Lagrangian, Eq. (1), if the mass term vanishes. An infinitesimal chiral transformation ($\mathrm{U}_A(1)$) is given by

$\psi' = (1 + i\epsilon\gamma_5)\psi$. Using $\psi_C = C\bar{\psi}^T$, we are lead to conclude, that $\psi'_C = (1 + i\epsilon\gamma_5)\psi_C$ and therefore

$$\mathcal{S}' = \begin{pmatrix} 1 + i\epsilon\gamma_5 & 0 \\ 0 & 1 + i\epsilon\gamma_5 \end{pmatrix} \mathcal{S} \begin{pmatrix} 1 + i\epsilon\gamma_5 & 0 \\ 0 & 1 + i\epsilon\gamma_5 \end{pmatrix}. \tag{100}$$

However, in a Nambu-Gor'kov space, we formally have two independent chiral transformations on ψ and ψ_C, describing the pairing of same and opposite chirality, respectively. We could therefore also require

$$\mathcal{S}' = \begin{pmatrix} 1 + i\epsilon\gamma_5 & 0 \\ 0 & 1 - i\epsilon\gamma_5 \end{pmatrix} \mathcal{S} \begin{pmatrix} 1 + i\epsilon\gamma_5 & 0 \\ 0 & 1 - i\epsilon\gamma_5 \end{pmatrix}. \tag{101}$$

Like chirality
For like chirality we require

$$\{\gamma_5, S\} = 0 \quad \text{and} \quad [\gamma_5, T] = 0. \tag{102}$$

Opposite chirality
For opposite chirality we require

$$\{\gamma_5, S\} = 0 \quad \text{and} \quad \{\gamma_5, T\} = 0. \tag{103}$$

4.2 Colour spin locking of massless quarks

First we compute the quark propagator in the CSL phase for massless quarks. This was done first, because the analysis for massless quarks uses only half the tensor structures that are needed in the massive case. Thus it is easier to investigate. Once we showed it to be working, it is a simple task to extend the analysis to massive quarks.
We will use the ansatz, Eq. (74), discussed in section 2.5 and impose chirality conditions.

The normal propagator S for massless quarks

For the normal propagator, we require $S(\vec{p}) = \gamma_4 S(-\vec{p})\gamma_4$ and $\{\gamma_5, S\} = 0$, cf. Eq. (98) and (103) respectively. This requirement can be fulfilled by the following tensor structures in colour-Dirac space, where $i, j \in \{1, 2, 3\}$ denote colour indices, the indices in Dirac space are suppressed:

$$\begin{aligned} P_{1,ij} &= \gamma_4 \delta_{ij} \\ P_{2,ij} &= \gamma_5\gamma_4 \left(\hat{p} \cdot \vec{\lambda}_{ij}\right) \\ P_{3,ij} &= i\gamma_5 \left(\vec{\gamma} \cdot \vec{\lambda}_{ij}\right) \\ P_{4,ij} &= \gamma_4 \left(\hat{p}_i \hat{p}_j\right) \\ P_{5,ij} &= \left(\gamma_i \hat{p}_j + \hat{p}_i \gamma_j\right). \end{aligned}$$

The quark propagator for massless quarks in the CSL phase is given by

$$S^+ = Z_2 \sum_{i=1}^{5} \left(S_{C,i} + i\gamma_4 \hat{\not{p}} S_{A,i}\right) P_i. \tag{104}$$

This constitutes the ten different ways of coupling the 'spins', confirming all possible couplings are realized. The selfenergy has the same structure:

$$\Sigma^+ = \frac{Z_2}{Z_{1F}} \sum_{i=1}^{5} \left(\Sigma_{C,i} + i\gamma_4 \hat{\not{p}} \Sigma_{A,i} \right) P_i. \tag{105}$$

The anomalous propagator T and the gap Φ for massless quarks

For the anomalous propagator, we require $T(\vec{p}) = -\gamma_4 T(-\vec{p})\gamma_4$ and $\{\gamma_5, T\} = 0$. This condition is easily satisfied by defining $M_i = \gamma_5 P_i$ and using these tensor structures to build up the anomalous propagator T and the gap Φ.

$$\begin{aligned}
M_{1,ij} &= \gamma_5\gamma_4\delta_{ij} \\
M_{2,ij} &= \gamma_4 \left(\hat{p} \cdot \vec{\lambda}_{ij} \right) \\
M_{3,ij} &= i \left(\vec{\gamma} \cdot \vec{\lambda}_{ij} \right) \\
M_{4,ij} &= \gamma_5\gamma_4 \left(\hat{p}_i \hat{p}_j \right) \\
M_{5,ij} &= \gamma_5 \left(\gamma_i \hat{p}_j + \hat{p}_i \gamma_j \right),
\end{aligned}$$

With these definitions the anomalous propagator and the gap have the structure

$$T = Z_2 \sum_{i=1}^{5} \left(T_{C,i} + i\gamma_4 \hat{\not{p}} T_{A,i} \right) M_i. \tag{106}$$

$$\Phi = \frac{Z_2}{Z_{1F}} \sum_{i=1}^{5} \left(\phi_{C,i} + i\gamma_4 \hat{\not{p}} \phi_{A,i} \right) M_i. \tag{107}$$

The algebra

Having chosen a tensor structure for our ansatz, we need to see if the algebra closes, in particular to determine, what products of structures lie in the chosen basis. This is done using Mathematica and all products turned out, to lie in the algebra, thus the algebra closes. This is necessary for the ansatz to be selfconsistent.

Solving the DSE for the quark propagator

To solve the DSE for the quark propagator we proceed in several steps. We start with a bare quark propagator and introduce a small perturbation into the quark propagator by setting the gap functions to constant values that are close to their expected final peak values. Then we solve the gap equations, Eq. (61) iteratively.
The first step in the iteration is to compute an updated value for the selfenergy, which is then used to compute $((S_0^-)^{-1} + \Sigma^-)^{-1}$. We get the anomalous propagator using Eq. (55). It is used in the gap equation to get an updated value for the gap functions.
Having computed an updated value for the gap functions we use these to compute the inverse quark propagator via Eq. (55) and invert it. After that the procedure starts over again until an approximate fixpoint of the equation is reached.

Inversion of the propagator

The inversion of the normal propagator is very important for solving the coupled system of equations. Unfortunately it is merely impossible to compute this analytically, but it can be done numerically using an LU decomposition. To check for the accuracy of the inversion we compared the results in different limiting cases of the full ansatz with the previously obtained analytic results and deviations are indiscernible.
The idea is to multiply two propagators S_1, S_2 and see how the coefficient functions are related if we set the product equal to the identity operator. Therefore we define $S_Q = \sum_{i=1}^{5} \left(S_{Q,C,i} + i\gamma_4 \hat{\not{p}} S_{Q,A,i} \right) Q_i$ where $Q_i = \gamma_4 P_i$, i.e.

$$\begin{aligned} Q_{1,ij} &= \delta_{ij} \\ Q_{2,ij} &= -\gamma_5 \left(\hat{p} \cdot \vec{\lambda}_{ij} \right) \\ Q_{3,ij} &= i\gamma_4\gamma_5 \left(\vec{\gamma} \cdot \vec{\lambda}_{ij} \right) \\ Q_{4,ij} &= (\hat{p}_i \hat{p}_j) \\ Q_{5,ij} &= \gamma_4 \left(\gamma_i \hat{p}_j + \hat{p}_i \gamma_j \right). \end{aligned}$$

We take the product of the two propagators S_1, S_2 and determine the functions $S_{Q,C,i}$ and $S_{Q,A,i}$ if we set $S_1 \cdot S_2 = S_Q$.
From this we get a system of equations for the coefficients, where we set $S_{Q,C,i} = 1$ and all other components to zero. Solving this set for the coefficients $S_{2,C,i}$ and $S_{2,A,i}$ we get S_2 which is the inverse normal propagator of S_1.

Results

The results for the scalar gap functions are shown in Fig. 14, where we plotted only the results for the four large scalar gap functions. The other scalar gap functions are several orders of magnitude smaller. This is not surprising since these scalar gap functions are only induced by the Cooper pairing in the attractive channel.
The ansatz for the gap function in section 3, Eq. (76), in the transverse case corresponds to setting $\phi_{A,2} = \phi_{C,3}, \phi_{A,3} = \phi_{C,2}$ and all other scalar gap function to zero. We see that

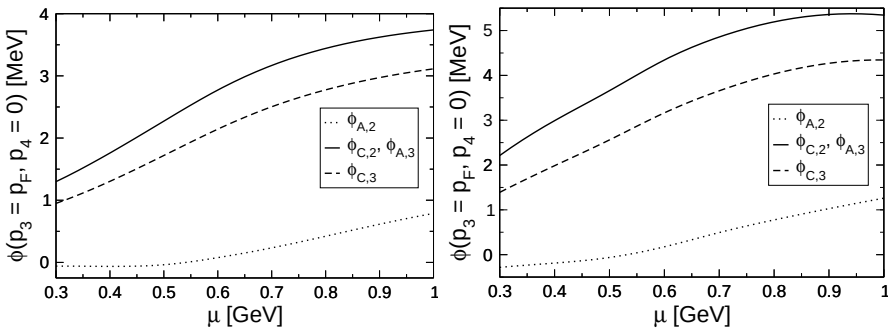

Figure 14: The values of the gap functions at the Fermi surface for the two most important tensor structures in the case of massless quarks. The left graph shows the results using the effective strong running coupling α_I, the right graph shows the results using α_{II}

a selfconsistent colour-spin structure is different from the one used in section 3.

4.3 Colour spin locking of massive quarks

Now we turn to the case of massive quarks. We will employ the same formalism developed in the previous section, but allowing for massive quarks. The case of massive quarks is of special interest because for neutron star phenomenology it could have important implications. This is because we expect no gapless modes in the excitation spectrum for massive quarks (cf. [17]), whereas we found gapless modes in the massless case. A detailed discussion of the excitation spectrum of quarks in the CSL phase is presented in the next section. We are also interested in the question whether there is a spontaneous breaking of chiral symmetry in CSL phase. Including quark masses also means that these masses have to be renormalised. The quark masses given in the particle data book [32] are computed using the $\overline{\text{MS}}$ renormalisation scheme. By contrast we work in a MOM renormalisation scheme. Therefore the quark masses used here might not coincide with the corresponding quark masses in the particle data book. However, the differences in the renormalised quark mass between the two renormalisation schemes is negligible compared to the experimental uncertainties in the particle data book. In addition we will also investigate the influence of the quark mass on the scalar gap functions. If this influence is rather small we can safely employ our MOM renormalisation scheme to renormalise the quark mass.

The normal propagator S for massive quarks

To allow for massive quarks we have to drop the requirement of chirality. Thus we only require for the normal propagator $S(\vec{p}) = \gamma_4 S(-\vec{p})\gamma_4$. Note that we simply dropped the requirement that the propagator has to anticommute with γ_5.
Imposing chirality enabled us to drop half of the terms allowed by CSL symmetry and parity. These have to be included for a calculation with massive quarks. This can easily be realized by keeping the tensor structures P_i and M_i and replace

$$X_{C,i} + i\gamma_4\hat{\not{p}}X_{A,i} \to X_{C,i} + i\gamma_4\hat{\not{p}}X_{A,i} + \gamma_4 X_{B,i} + i\hat{\not{p}}X_{D,i}, \tag{108}$$

where X can be any of the objects S, Σ, T, ϕ.
The quark propagator for massive quarks in the CSL phase is then given by

$$S^+ = Z_2 \sum_{i=1}^{5} \left(S_{C,i} + i\gamma_4\hat{\not{p}}S_{A,i} + \gamma_4 S_{B,i} + i\hat{\not{p}}S_{D,i}\right) P_i. \tag{109}$$

The selfenergy has the same structure:

$$\Sigma^+ = \frac{Z_2}{Z_{1F}} \sum_{i=1}^{5} \left(\Sigma_{C,i} + i\gamma_4\hat{\not{p}}\Sigma_{A,i} + \gamma_4 \Sigma_{B,i} + i\hat{\not{p}}\Sigma_{D,i}\right) P_i. \tag{110}$$

The anomalous propagator T and the gap Φ for massive quarks

For the anomalous propagator, we now only require $T(\vec{p}) = -\gamma_4 T(-\vec{p})\gamma_4$, this condition is again easily satisfied by defining $M_i = \gamma_5 P_i$ and using these tensor structures to build the anomalous propagator T and the gap Φ.
Following the prescription, Eq. (108) and using the definitions for M_i the anomalous propagator and the gap have the structure

$$T = Z_2 \sum_{i=1}^{5} \left(T_{C,i} + i\gamma_4 \hat{\not{p}} T_{A,i} + \gamma_4 T_{B,i} + i\hat{\not{p}} T_{D,i} \right) M_i. \tag{111}$$

$$\Phi = \frac{Z_2}{Z_{1F}} \sum_{i=1}^{5} \left(\phi_{C,i} + i\gamma_4 \hat{\not{p}} \phi_{A,i} + \gamma_4 \phi_{B,i} + i\hat{\not{p}} \phi_{D,i} \right) M_i. \tag{112}$$

Solving the DSE using this parametrisation is completely analogous to the massless case.

4.4 Results for massive quarks using α_I

First we will discuss the results that were obtained using the effective strong running coupling α_I. The behaviour of the scalar gap functions as functions of μ is shown in Fig. 15. Here we focus only on the scalar gap functions to the tensor structures P_2 and P_3. These correspond to the attractive colour channel and will be significantly larger than the other scalar gap functions. The scalar gap functions $\phi_{A,i}$ and $\phi_{C,i}$ coincide quite well with the ones obtained in the massless case. The other scalar gap $\phi_{B,i}$ and $\phi_{D,i}$ functions did of course not appear in the analysis of the massless case.
As pointed out before, we are interested in the effect of the quark mass on the scalar gap functions. Fig. 16 shows the values of the gap functions at the Fermi surface for various quark masses. There we can nicely see that for small chemical potential μ the gap functions $\phi_{B,2}$ and $\phi_{D,2}$ depend strongly on the quark mass, whereas the gap functions $\phi_{A,2}$ and $\phi_{C,2}$ are nearly independent of the quark mass. At higher chemical potential,

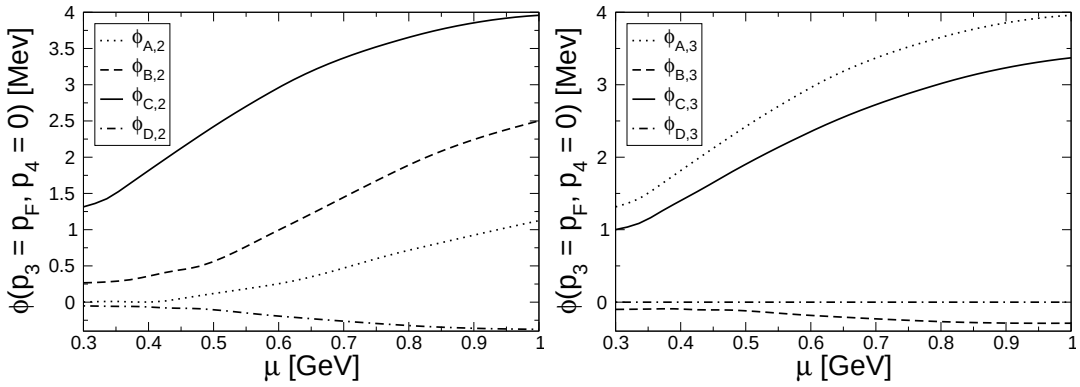

Figure 15: The values of the gap functions $\phi_{A,B,C,D;2,3}$ at the Fermi surface for massive quarks with a renormalised quark mass of 18.4 MeV at the renormalisation point $\nu = 2$ GeV

the dependence of $\phi_{B,2}$ and $\phi_{D,2}$ on the quark mass is relatively weak. That the functions $\phi_{B,i}$ and $\phi_{D,i}$ depend on the quark mass is not surprising since they are related to chiral symmetry breaking. Unexpected is that the scalar gap functions $\phi_{B,2}$ and $\phi_{D,2}$ are finite even at vanishing quark masses. This will be very important for the excitation spectrum, since all excitation modes will be gapped for non-vanishing $\phi_{B,2}$ (cf. Section 5).
The dependence of the size of the gaps is also shown in Fig. 18. Again we can clearly see the effect of the quark masses on the scalar gap functions $\phi_{B,i}$ and $\phi_{D,i}$.
Because for compact star phenomenology the region of chemical potentials between 300 and 500 MeV is most interesting, we want to show this region in more detail. The values of the gap functions at the Fermi surface are shown in Fig. 17. Here we see a wiggling in some of the curves, this is because the gaps are very small and are therefore numerically difficult to handle. The dominating scalar gap functions, however, show a more regular behaviour.

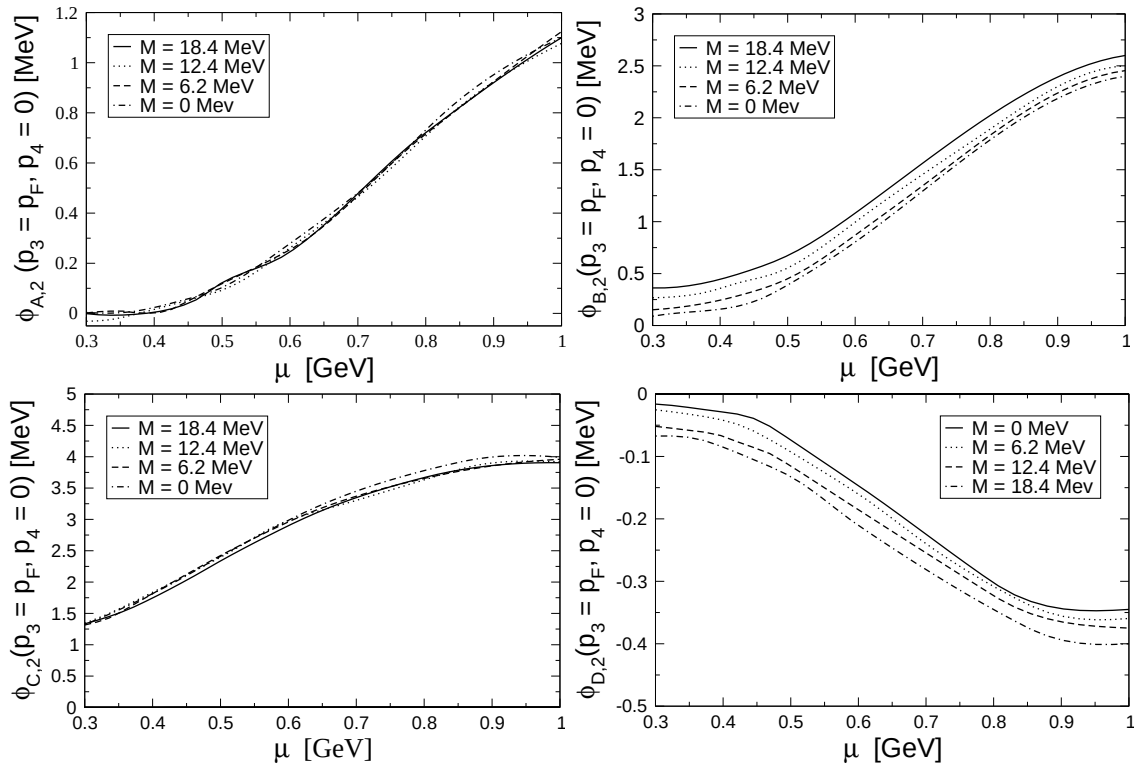

Figure 16: The values of the gap functions $\phi_{A,B,C,D;2}$ at the Fermi surface for different renormalised quark masses at the renormalisation point $\nu = 2$ GeV, plotted as a function of chemical potential μ.

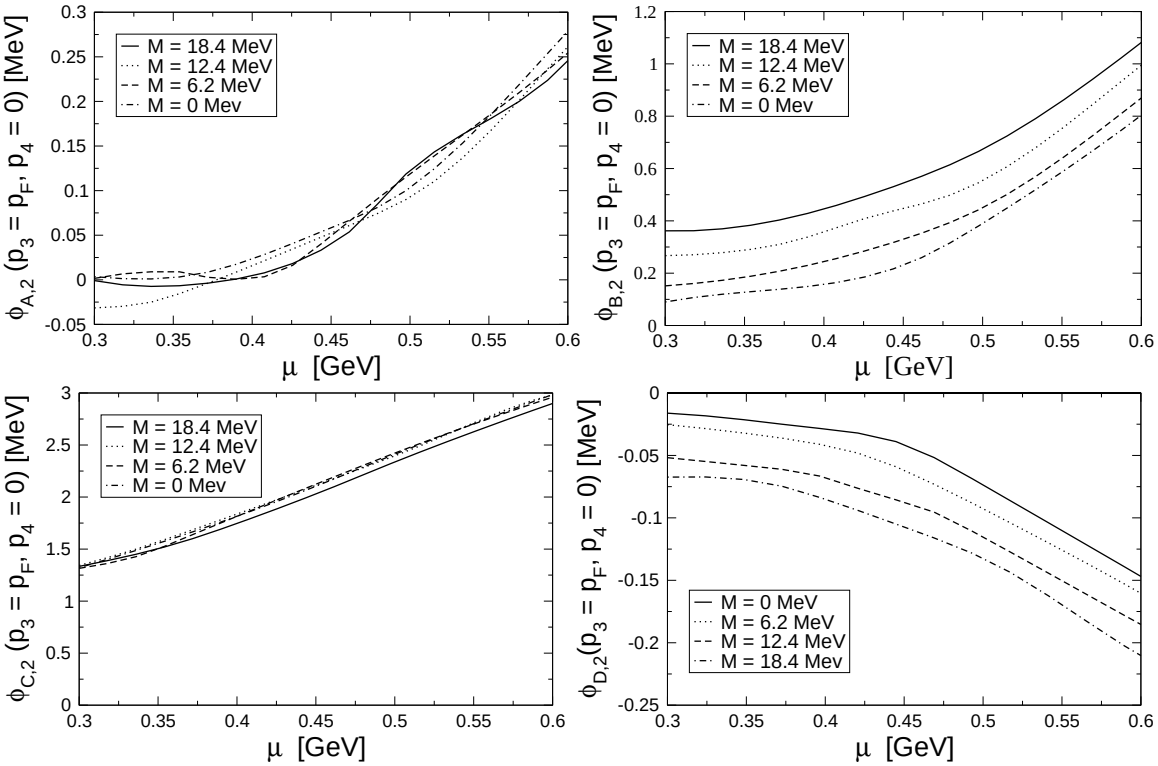

Figure 17: The values of the gap functions $\phi_{A,B,C,D;2}$ at the Fermi surface for different renormalised quark masses at the renormalisation point $\nu = 2$ GeV, plotted as a function of chemical potential μ.

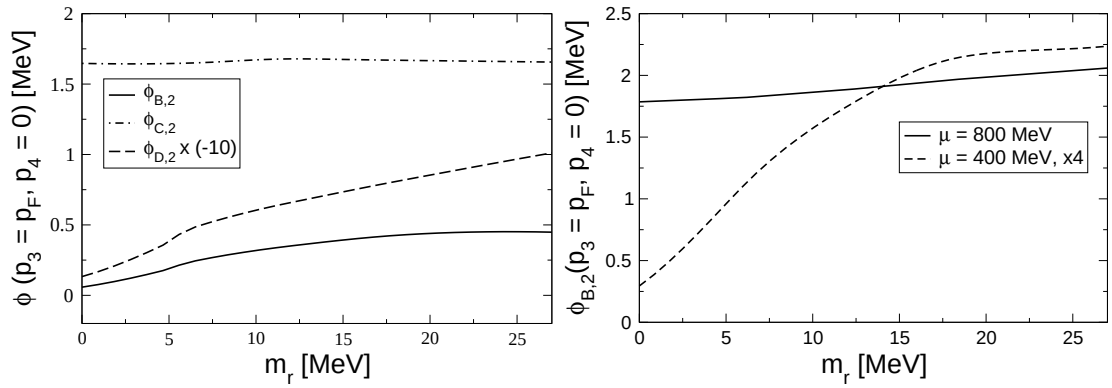

Figure 18: The effect of the quark mass on the scalar gap functions. The left graph shows how the value of the scalar gap functions $\phi_{B,2}$, $\phi_{C,2}$ and $\phi_{D,2}$ at the Fermi surface behaves for a chemical potential $\mu = 400$ MeV. Because the value for $\phi_{D,2}$ is one order of magnitude smaller than the other two functions we multiplied it by -10. The right graph shows only the values of $\phi_{B,2}$ at the Fermi surface, here the behaviour is shown for different chemical potentials. We multiplied the values of $\phi_{B,2}$ at the Fermi surface by 4 for $\mu = 400MeV$. The renormalisation point is $\nu = 2$ GeV.

4.5 Results for massive quarks using α_{II}

We are now going to investigate the solutions of the quark DSE using the effective strong running coupling α_{II}. Compared to the results obtained using α_I the results differ only quantitatively, therefore, we are only going to show the analogous figures to the figures we showed above and comment on the differences.
Fig. 19 shows the gap functions at the Fermi surface as a function of chemical potential for the two most important tensor structures. It is interesting that for chemical potentials of about 1 GeV the gap function $\phi_{B,2}$ gets larger than $\phi_{C,2}$. This is different from the previous results for the effective strong running coupling α_I. Also the values of the scalar gap functions at the Fermi surface are generally larger than in the case where we used α_I. This is not surprising since α_{II} yielded a stronger chiral symmetry breaking in the infrared, therefore, we also expected it to generate larger scalar gap functions.
Again we are interested in the dependence of the gap functions on the quark masses. The gap functions at the Fermi function as a function of chemical potential are shown in Fig. 20 and 21. What we can see is that there is again a dependence of $\phi_{B,2}$ and $\phi_{D,2}$ on the quark mass, however, it is much less pronounced than in the previous case.

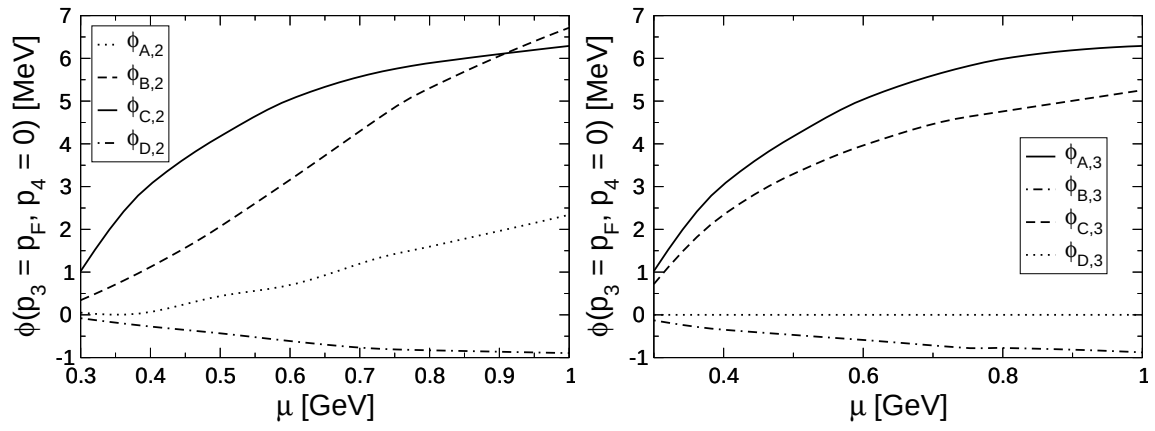

Figure 19: The scalar gap functions $\phi_{A,B,C,D;2,3}$ for a renormalised quark mass of 18 MeV at the renormalisation point $\nu = 2$ GeV.

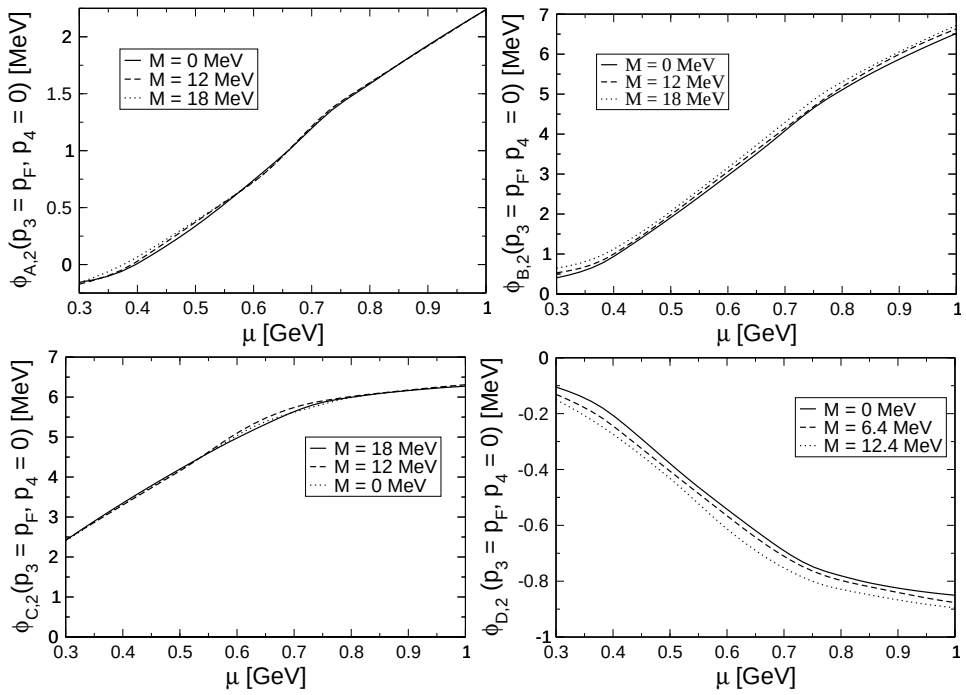

Figure 20: The gap functions $\phi_{A,B,C,D;2,3}$ for different renormalised quark masses at the renormalisation point $\nu = 2$ GeV, plotted as a function of chemical potential μ.

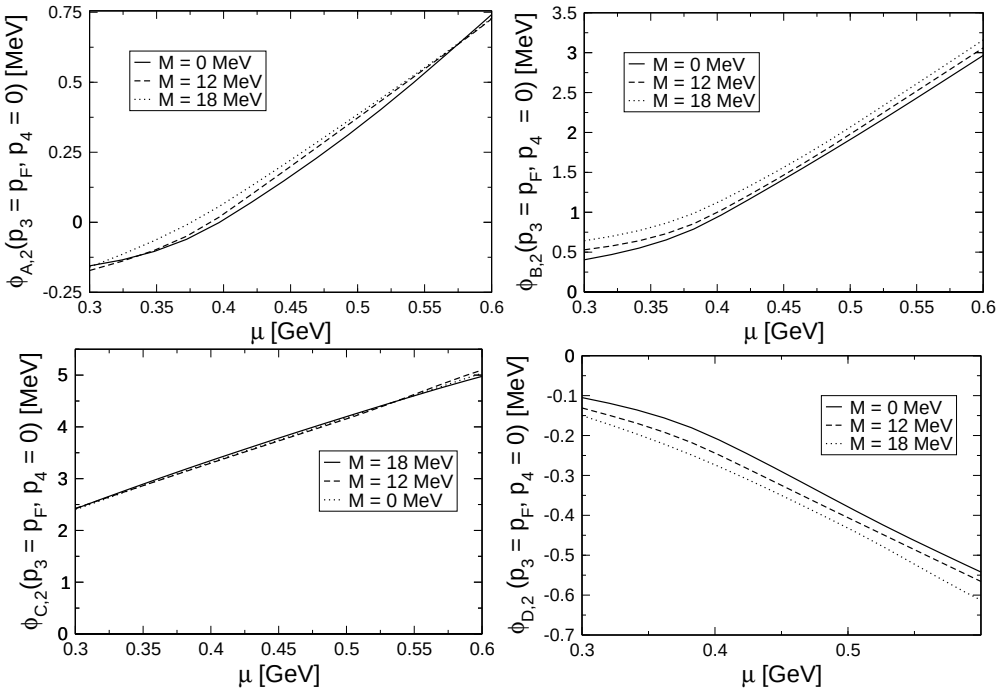

Figure 21: The gap functions $\phi_{A,B,C,D;2,3}$ for different renormalised quark masses at the renormalisation point $\nu = 2$ GeV, plotted as a function of chemical potential μ.

5 Dispersion relations

A dispersion relation is the relation between the free energy of an excitation and its corresponding momentum. We are going to study the dispersion relations of the quasiparticles and quasiholes in the CSL phase. If there is an energy gap between the quasiparticle and the quasihole dispersion relation, the corresponding excitation mode is called gapped. There are two qualitatively different types of excitation spectra in colour superconductivity, excitation spectra that consist of (a) only gapped excitation modes or (b) one or more ungapped modes. An example is shown in Fig. 22, the right panel shows type (a) and the left panel shows type (b), only positive free energies are shown.
In the case of an ungapped mode the free energy $\varepsilon(p)$ of that modes is of the type $\varepsilon(p) = \pm\sqrt{(p+e\mu)^2}$, where p is the absolute value of the three-momentum. For $e = -1$ modes of positive free energy correspond to quasiparticle excitations, modes of negative free energy to quasi-hole excitations. A dispersion relation with $e = +1$ corresponds to quasi-antiparticle and quasi-antihole excitations.
For a gapped mode the free energy is of the form $\varepsilon(p) = \pm\sqrt{(p+e\mu)^2 + \Delta_{eff}^2}$, where $e = \pm 1$ and Δ_{eff} is called the effective gap. In the excitation spectrum the energy gap is $2\Delta_{eff}$. The nomenclature is like in the case of an ungapped mode.
We are especially interested in the size of the smallest energy gap in the excitation spectrum, in particular if there is an ungapped mode or not. Only an estimate of the size of the energy gap is possible. The reason is that we work in Euclidean spacetime and have no direct connection Minkowski spacetime. Since dispersion relations are defined by the pole of the full quark propagator in Minkowski spacetime, we have to make some approximations to gain access to this pole. The problem lies in performing the analytic continuation of the selfenergies into Minkowski spacetime.

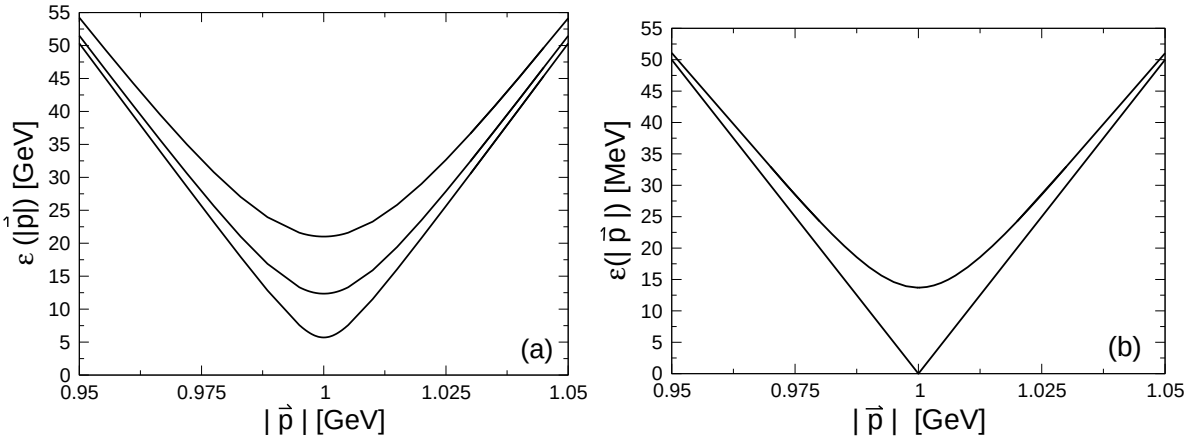

Figure 22: Examples of excitation spectra. The left graph shows the three different excitation modes of an excitation spectrum of type (a), i.e. containig only gapped modes. The right graph shows the two (partly degenerate) excitation modes of an excitation spectrum of type (b), i.e. containing an ungapped mode.

5.1 Previous investigations

As already pointed out, the question whether there is an ungapped mode in the excitation spectrum or not, is of special interest. We will consider the results for the gap functions that we obtained from the ansatz for the gap matrix, Eq. (112) for massive quarks and Eq. (107) for massless quarks. The dispersion relations for massive quarks in the CSL phase have been investigated in [17] and [33]. The authors of [33] used a DSE approach in the weak coupling limit. Their ansatz for the gap function can be translated into our ansatz in Eq. (112). This is achieved by setting

$$\phi_{C,3} = \phi_{A,2} \quad , \tag{113}$$

and all other scalar gap functions to zero, which is not selfconsistent. The authors found that there is an ungapped mode in the excitation spectrum just as in the massless case of the CSL phase, investigated in [16].
In an NJL type model investigation [17] it was found that there are only gapped modes in the excitation spectrum and that the smallest effective gap is given by

$$\Delta_{eff} = \frac{M}{\sqrt{\mu^2 + \Delta^2}}\Delta, \tag{114}$$

where M is the quark mass, μ is the quark chemical potential and Δ is the gap parameter, which in this type of model is proportional to the diquark condensates, Eq. (67). In this investigation the quark mass is dynamically generated even for small current quark masses. This is a remarkable contrast, for one work states that the current quark mass does not qualitatively influence the excitation spectrum [33]. Whereas in the other work the current quark mass is of utmost importance to the question on the existence of ungapped modes in the excitation spectrum.
Now the scene for our investigation is set. First we will investigate the excitation spectrum for massless quarks ($M = 0$) using the ansatz, Eq. (107), to get an idea of the excitation spectrum. Then we will consider the full ansatz in Eq. (112) first for massive quarks ($M \neq 0$) and also for massless quarks ($M = 0$). To conclude we will analyse the excitation spectrum obtained by constraining the ansatz for the gap function to the one in Eq. (113), keeping a mass term in the quark propagator ($M \neq 0$).

5.2 Obtaining the dispersion relations

The dispersion relations are obtained as a solution to the algebraic equation

$$0 = \mathrm{Det}[\mathcal{S}^{-1}] = \mathrm{Det}\left[\begin{pmatrix} (S_0^+)^{-1} & \Phi^- \\ \Phi^+ & (S_0^-)^{-1} \end{pmatrix}\right] \tag{115}$$

for ip_4 at a given 3-momentum $\vec{p}$. The quasiparticle excitation energy is obtained by setting $E(|\vec{p}|) = ip_4$, where $\mathrm{Det}[\mathcal{S}^{-1}(p4, |\vec{p}|)] = 0$. We neglect the influence of the normal self-energy for the quarks and replace the scalar gap functions in $\Phi^{\pm}$ by their values at the Fermi surface.
The inverse propagator has a 24×24 matrix structure and the resulting equation cannot be handled analytically. Instead we search numerically for solutions to Eq. (115). For a given absolute value of the 3-momentum we expect three maybe degenerate solutions. These solutions belong to different branches of the quasiparticle excitation spectrum.

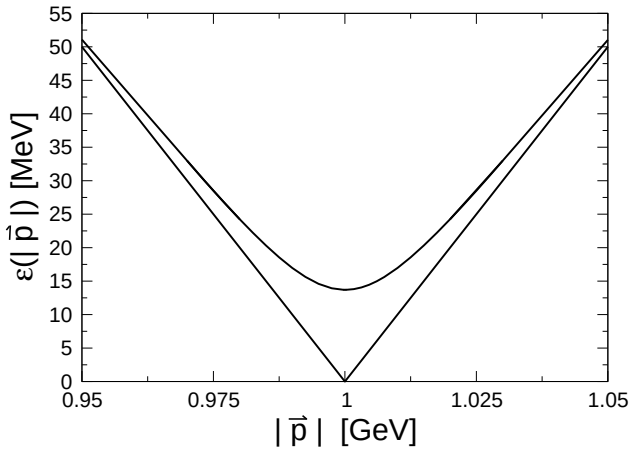

Figure 23: Excitation energies for massless quarks for $\mu = 1$ GeV

5.3 $M = 0$, $\phi_{B,i} = \phi_{D,i} = 0$

Fig. 23 shows the excitation spectrum for a chemical potential $\mu = 1$ GeV. The x-axis shows the absolute value of the 3-momentum $|\vec{p}|$ and the y-axis shows $\varepsilon(|\vec{p}|)$. If one of the branches of the excitation energy goes to zero at a certain absolute value of the 3-momentum $|\vec{p}|$, we have an ungapped mode. In Fig. 23 this seems to be the case. A carefull investigation confirms that there is an ungapped mode.

5.4 $M \neq 0$, $\phi_{B,i} \neq 0$, $\phi_{D,i} \neq 0$

In the previous section we investigated the excitation spectrum of quarks obtained from a selfconsistent solution of the DSE for massless quarks in the CSL phase. Now we want to explore the excitation spectrum of massive quarks using the full gap ansatz for the CSL phase, Eq. (112). Fig. 24 shows the result for massive quarks with a renormalised mass of $M = 18$ MeV, at the renormalisation point $\nu = 2$ GeV, for various chemical potentials. We observe that there are only gapped modes in the excitation spectrum.
Of interest for compact star cooling phenomenology is the behaviour of the size of the smallest effective gap as a function of chemical potential. This is shown in Fig. 25 for the effective strong running coupling α_{II} and in Fig. 26 for α_I. It mainly follows the size of the gap functions at the Fermi surface. This does not come as a surprise, since the full propagator is at the Fermi surface strongly dependent on the gap functions (cf. section 3). We also see that the size of the smallest effective gap differs roughly by a factor 2 between the different effective strong running couplings. More important, however, is that the difference is only quantitative, but not qualitative.
In addition we observe that the dependence of the effective gap on the quark masses is weak, particullarly for higher values of the chemical potential. Moreover does the smallest effective gap not seem to go to zero if we let the mass go to zero. Consequently we investigate the ansatz in Eq. (112) for zero current quark mass.

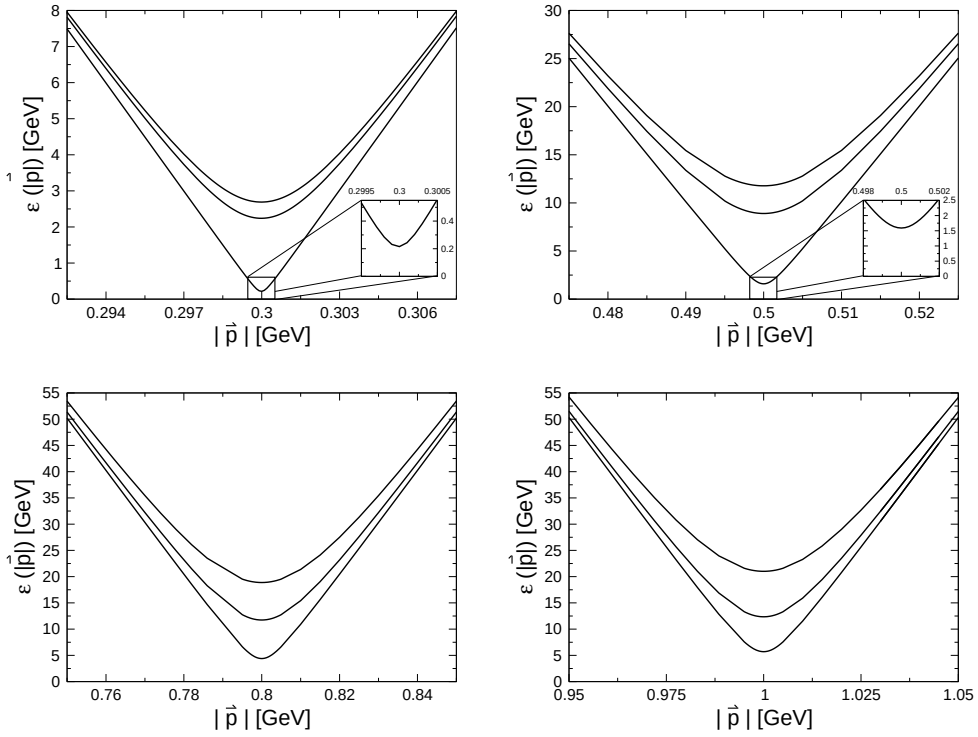

Figure 24: The excitation spectra for massive quarks (renormalised mass $M = 18$ MeV) at various chemical potentials μ. The upper left panel shows the excitation spectrum for $\mu = 300$ MeV, the upper right for $\mu = 500$ MeV, the lower left for $\mu = 800MeV$ and the lower right for $\mu = 1000$ MeV. The plot shows the excitation energies as a function of the absolute value of the 3-momentum $|\vec{p}|$. The effective strong running coupling is α_{II}.

5.5 $M = 0$, $\phi_{B,i} \neq 0$, $\phi_{D,i} \neq 0$

We already found that the excitation spectrum of massive quarks exhibits only gapped modes. Preceeding this observation, we discovered that quarks in the chiral limit have an ungapped mode in the excitation spectrum, but this analysis neglected the possibility of massless quarks having nonvanishing scalar gap functions ϕ_B or ϕ_D. These terms can and will induce chiral symmetry violating terms in the quark propagator.
The analysis including ϕ_B and ϕ_D reveals that there are again only gapped modes in the excitation spectrum. The resulting smallest effective gap in the excitation spectrum as a function of chemical potential is shown in Fig. 25 for the effective strong running coupling α_{II} and in Fig. 26 for α_I.
It turns out that the scalar gap functions ϕ_B and ϕ_D are more important for the excitation spectrum than the current quark mass. This is a novel feature that could not be expected from the previous investigation of the excitation spectrum of the CSL phase.

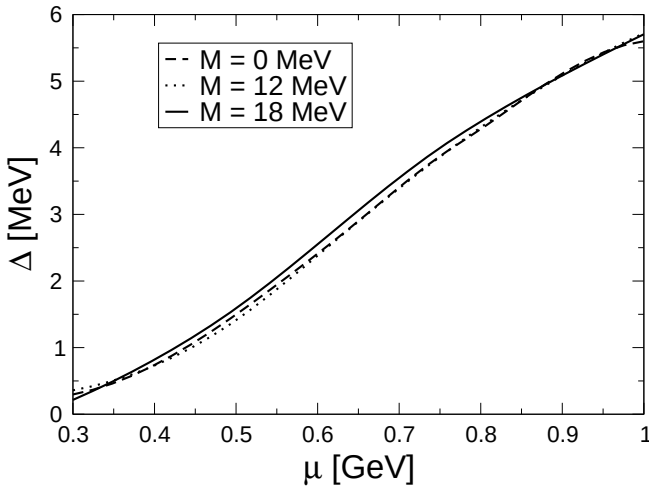

Figure 25: The smallest effective gap in the excitation spectrum Δ as a function of chemical potential μ for massive quarks. The effective strong running coupling is α_{II}.

5.6 $M \neq 0$, $\phi_{B,i} = \phi_{D,i} = 0$

As pointed out at the beginning of this section, from the analysis in [33] it is expected that there is an ungapped mode in the excitation spectrum if we restrict the ansatz for the gap matrix to Eq.(113). This is also the result of our analysis in section 3, however, such an ansatz is not selfconsistent. Nevertheless, we mention that doing a similar analysis by selfconsistently solving the gap equation, Eq. (61), setting $\phi_{B,i} = \phi_{D,i} = 0,\ i \in 1, \ldots, 5$, it turns out that there is an ungapped mode in the excitation spectrum.

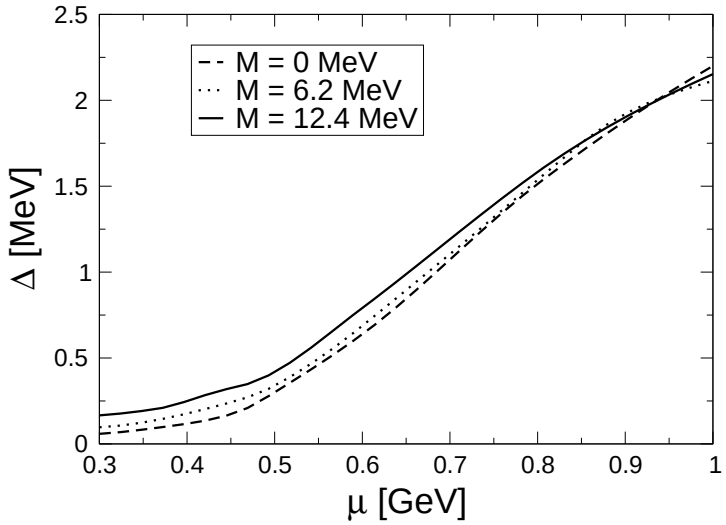

Figure 26: The smallest effective gap in the excitation spectrum Δ as a function of chemical potential μ for massive quarks. The effective strong running coupling is α_I.

6 Summary and outlook

The subject of this thesis has been the quark propagator in the colour-superconducting CSL phase. It has recently been investigated in the weak coupling limit and also in an NJL type model of QCD. The colour-spin locked phase is interesting because it might be the phase being realised in the interior of compact stars, since other phases might become disfavoured due to neutrality conditions.
We aimed for a fully self-consistent solution of the DSE for the quark propagator in the abelian approximation. This included dynamically determining the colour-spin structure of the gap function rather than having to resort to an arbitrarily chosen ansatz. In our approximation scheme we employed two different interactions, that can be viewed as opposing, limiting cases of the QCD interaction. Using different interactions, we can determine how sensitive the colour-spin locked phase is to our approximation of the DSE. It turned out that the sensitivity is rather weak.
We found that the CSL-phase exhibits a colour-spin structure that is in the chiral limit close to the colour-spin structure used in weak coupling calculations [16]. Yet, the full colour-spin structure of the quark propagator is richer because of the chiral symmetry violating terms. These terms can be dynamically generated, which is energetically favoured, and turn out to be import for the excitation spectrum. It seems worthwhile to repeat the analysis of the CSL phase in the NJL type model including terms of this sort. In this context it would be interesting to see if the influence of the current quark masses is still as dominant as it was before.
The terms mentioned above did not only appear for finite current quark mass, but are generated dynamically. Moreover, their dependence on the current quark mass is rather weak. This is advantageous since we do not have to worry about the different renormalisation schemes, that the quark masses depend on.
Concluding our analysis, we determined the excitation spectrum for quarks in the colour-spin locked phase. We focused on the smallest effective energy gap in the excitation spectrum. Contrasting this with previous investigations of the excitation spectrum of quarks in the colour-spin locked phase, we found that the smallest effective gap is mainly driven by the gap function and only weakly dependent on the current quark masses. In the previous investigations the current quark masses either did not qualitatively change the excitation spectrum or were equally important as the gap function, and therefore have to be retained in the calculation.

Our investigation of the colour-spin locked phase could be refined in various directions. One direction would be to relax some of the approximations being used. In Eq. (39) we could use functions F and G that are computed using dressed instead of bare quark propagators, this is know as quasiparticle-random-phase-approximation. Another desirable improvement would be a better vertex approximation, Eq. (28). Advancing in another direction it would be interesting to explore the behaviour of the superconducting state for finite temperature. Finally one could also think about other spin-1 colour-superconducting phases, like the A-phase. This phase is even more intricate, since it is not spatially isotropic.

A Conventions

We will use the following conventions throughout this work, following the conventions used in [34]

- The metric $g_{\mu\nu}$ that defines the inner product of two 4-vectors is Euclidian in all calculations:

$$g_{\mu\nu} = \delta_{\mu\nu}, \tag{116}$$

  where $\delta_{\mu\nu}$ is the Kronecker symbol. Consequently we do not need to distinguish between covariant and contravariant tensor structures.

- We work in natural units where

$$\hbar = c = 1.$$

- We use the Einstein sum convention.

- We use Euclidian gamma matrices. They are related to gamma matrices in Minkoski space via, see e.g. [35]

$$\gamma_4^E = \gamma_0^M \ , \ \gamma_a^E = -i\gamma_a^M \ \ a = 1,2,3 \ , \ \gamma_5^E = -\gamma_1^E\gamma_2^E\gamma_3^E\gamma_4^E. \tag{117}$$

- Greek indices run from 1 to 4.

- Latin indices run from 1 to 3.

B Derivation of the unrenormalised DSE for the quark propagator

To get the quark Dyson-Schwinger equation we start by taking a functional derivative on the generating functinal, Eq.(13), with respect to $\bar{\psi}$

$$\begin{aligned} 0 &= \int \mathcal{D}A\mathcal{D}\bar{\psi}\mathcal{D}\psi\mathcal{D}\bar{c}\mathcal{D}c \frac{\delta}{\delta\bar{\psi}(x)} \exp\left[-S_{QCD} - S_{gf} + S_{source}\right] \\ &= \int \mathcal{D}A\mathcal{D}\bar{\psi}\mathcal{D}\psi\mathcal{D}\bar{c}\mathcal{D}c \left[\frac{\delta S_{QCD}}{\delta\bar{\psi}(x)} + \eta(x)\right] \exp\left[-S_{QCD} - S_{gf} + S_{source}\right] \\ &= \left[\frac{\delta S_{QCD}}{\delta\bar{\psi}(x)}\left(\frac{\delta}{i\delta J^{\mu}_{A}(x)}, \frac{\delta}{i\delta\bar{\eta}(x)}, -\frac{\delta}{i\delta\eta(x)}\right) + \eta(x)\right] Z(J,\eta,\bar{\eta}) \\ &= \left[\eta(x) + \left(\not{\partial} - \gamma_4\mu - m + ig\gamma^{\mu}t_a\frac{\delta}{i\delta J^{a}_{\mu}(x)}\right)\frac{\delta}{i\delta\bar{\eta}(x)}\right] Z(J,\eta,\bar{\eta}). \end{aligned} \tag{118}$$

Following this step we apply a derivative with respect to η, $\delta/\delta\eta(y)$, yielding

$$0 = \delta^4(x-y)Z - \left(\not{\partial} - \gamma_4\mu - m + ig\gamma^{\mu}t_a\frac{\delta}{i\delta J^{a}_{\mu}(x)}\right)\frac{\delta}{i\delta\eta(y)}\frac{\delta}{i\delta\bar{\eta}(x)}Z. \tag{119}$$

To proceed we switch from the generating functional for complete n-point Green functions $Z(J,\eta,\bar{\eta})$ to the generating functional for "connected" n-point Green functions, $W(J,\eta,\bar{\eta})$. These two functionals are related via

$$Z(J,\eta,\bar{\eta}) \equiv \exp\{iW(J,\eta,\bar{\eta})\} \tag{120}$$

Using this generating functional we can obtain a natural definition of the connected quark two-point function $S(x,y;[A^a_\mu])$ in an interacting theory:

$$S(x,y;[A^a_\mu]) = -\frac{\delta^2 W}{\delta\eta(y)\delta\bar{\eta}(x)} = \frac{\delta^2 W}{\delta\bar{\eta}(x)\delta\eta(y)}. \tag{121}$$

For a theory of free fermions this definition reproduces the Feynmann propagator.
The derivative on the right hand side of Eq. (121) is also implicitly present in Eq. (119), because with Eq. (120) we get the relation

$$\begin{aligned} \frac{\delta^2 Z}{i\delta\eta(y)\; i\delta\bar{\eta}(x)} &= \frac{\delta^2}{i\delta\eta(y)\; i\delta\bar{\eta}(x)}\exp(iW) = \frac{\delta}{i\delta\eta(y)}\left[\frac{\delta W}{i\delta\bar{\eta}(x)}\exp(iW)\right] \\ &= \left[i\frac{\delta^2 W}{i\delta\eta(y)\; i\delta\bar{\eta}(x)} - \frac{\delta W}{i\delta\bar{\eta}(x)}\frac{\delta W}{i\delta\eta(y)}\right]\exp(iW). \end{aligned} \tag{122}$$

At the end of the calculation we want to set the source terms to zero. Then the term containing only first derivatives vanishes, because the derivative terms are vacuum expectation values of the fields ψ and $\bar{\psi}$. So we omit the second term in brackets on the right hand side of Eq. (122) for the rest of the analysis.
After setting $\eta = 0 = \bar{\eta}$, the Dyson-Schwinger equation is

$$\begin{aligned} 0 &= \delta^4(x-y)Z - \left(\not{\partial} - \gamma_4\mu - m + ig\gamma^{\mu}t_a\frac{\delta}{i\delta J^{a}_{\mu}(x)}\right) Z\; S(x,y;[A^a_\mu]) \\ &= \delta^4(x-y)Z - Z\left(\not{\partial} - \gamma_4\mu - m + ig\gamma^{\mu}t_a A^a_\mu + ig\gamma^{\mu}t_a\frac{\delta}{i\delta J^{a}_{\mu}(x)}\right) S(x,y;[A^a_\mu]). \end{aligned} \tag{123}$$

The gauge field A^a_μ vanishes in the absence of an external source J^a_μ. It only remains to evaluate

$$\frac{\delta S(x,y;[A^a_\mu])}{i\delta J^a_\mu(x)} = \int d^4z \frac{\delta A^\nu_b(z)}{i\delta J^\mu_A(x)} \frac{\delta S}{\delta A^\nu_b(z)} \tag{124}$$

Therefore, we first introduce a generating functional for one-particle-irreducible (1PI) Green functions, $\Gamma[A^a_\mu, \psi, \bar{\psi}]$. It is obtained from $W(J, \eta, \bar{\eta})$ via a Legendre transformation

$$W(J,\eta,\bar{\eta}) = \Gamma[A^a_\mu,\psi,\bar{\psi}] + \int d^4x \left[\bar{\psi}\eta + \bar{\eta}\psi + A^a_\mu J^a_\mu(x)\right] \tag{125}$$

A 1PI n-point function, also called "proper vertex", only contains contributions that do not become disconnected when a single propagator is removed, e.g. via functional differentiation. This functional obeys

$$\frac{\delta W}{\delta\bar{\eta}} = \psi \quad , \quad \frac{\delta W}{\delta\eta} = -\bar{\psi} \quad , \quad \frac{\delta W}{\delta J^\mu_a} = -A^a_\mu. \tag{126}$$

Using the chain rule we get the identy

$$\begin{aligned} -\int d^4z \, \frac{\delta^2 W}{\delta\eta(x)\delta\bar{\eta}(z)} \frac{\delta^2\Gamma}{\delta\psi(z)\delta\bar{\psi}(y)}\bigg|_{\eta=0=\bar{\eta},\ \psi=0=\bar{\psi}} &= \int d^4z \, \frac{\delta\psi(z)}{\delta\eta(x)} \frac{\delta\eta(y)}{\delta\psi(z)}\bigg|_{\eta=0=\bar{\eta},\ \psi=0=\bar{\psi}} \\ &= \frac{\delta\eta(y)}{\delta\eta(x)} = \delta^4(x-y). \end{aligned} \tag{127}$$

The result of multiplying this expression from the right with $\left(\frac{\delta^2\Gamma}{\delta\psi(y)\delta\bar{\psi}(w)}\right)^{-1}$ and integrating over y is

$$-\frac{\delta^2 W}{\delta\eta(x)\delta\bar{\eta}(w)}\bigg|_{\eta=0=\bar{\eta}} = \left(\frac{\delta^2\Gamma}{\delta\psi(x)\delta\bar{\psi}(w)}\bigg|_{\psi=0=\bar{\psi}}\right)^{-1}. \tag{128}$$

With this relation at hand Eq. (124) can be expressed by

$$\frac{\delta S(x,y;[A^a_\mu])}{i\delta J^a_\mu(x)} = \int d^4z \frac{\delta A^\nu_b(z)}{i\delta J^\mu_A(x)} \frac{\delta}{\delta A^\nu_b(z)} \left(\frac{\delta^2\Gamma}{\delta\psi(x)\delta\bar{\psi}(y)}\bigg|_{\psi=0=\bar{\psi}}\right)^{-1}. \tag{129}$$

To compute the derivative of the inverse we use a trick that is a generalisation of the matrix identity

$$\frac{dA(x)^{-1}}{dx} = -A^{-1}(x)\frac{dA(x)}{dx}A^{-1}(x).$$

The idea is to differentiate the identity and rearrange terms

$$\begin{aligned} 0 &= \int d^4v \frac{\delta}{\delta A^\nu_b(z)} \left\{ \frac{\delta^2\Gamma}{\delta\psi(w)\delta\bar{\psi}(v)} \left(\frac{\delta^2\Gamma}{\delta\psi(v)\delta\bar{\psi}(y)}\right)^{-1} \right\} \\ &= \int d^4v \left(\frac{\delta}{\delta A^\nu_b(z)} \frac{\delta^2\Gamma}{\delta\psi(w)\delta\bar{\psi}(v)}\right) \left(\frac{\delta^2\Gamma}{\delta\psi(v)\delta\bar{\psi}(y)}\right)^{-1} + \\ &\quad \int d^4v \frac{\delta^2\Gamma}{\delta\psi(w)\delta\bar{\psi}(v)} \frac{\delta}{\delta A^\nu_b(z)} \left(\frac{\delta^2\Gamma}{\delta\psi(v)\delta\bar{\psi}(y)}\right)^{-1}. \end{aligned} \tag{130}$$

Now we multiply from left with $\left(\frac{\delta^2\Gamma}{\delta\psi(x)\delta\bar{\psi}(w)}\right)^{-1}$ and integrate over w to get

$$\begin{aligned}\frac{\delta}{\delta A^\nu_b(z)}\left(\frac{\delta^2\Gamma}{\delta\psi(x)\delta\bar{\psi}(y)}\right)^{-1} &= \int d^4w d^4v \left\{\left(\frac{\delta^2\Gamma}{\delta\psi(x)\delta\bar{\psi}(w)}\right)^{-1}\cdot \right. \\ &\quad \left.\left(\frac{\delta}{\delta A^\nu_b(z)}\frac{\delta^2\Gamma}{\delta\psi(w)\delta\bar{\psi}(v)}\right)\left(\frac{\delta^2\Gamma}{\delta\psi(v)\delta\bar{\psi}(y)}\right)^{-1}\right\} \qquad (131)\\ &= \int d^4w d^4v \;\; S(x,w,[A^a_\mu])\left(\frac{\delta}{\delta A^\nu_b(z)}\frac{\delta^2\Gamma}{\delta\psi(w)\delta\bar{\psi}(v)}\right)S(v,y,[A^a_\mu]).\end{aligned}$$

The term in brackets is the proper quark-gluon vertex:

$$\Gamma^b_\nu(w,v,z) \equiv \frac{\delta}{\delta A^\nu_b(z)}\frac{\delta^2\Gamma}{\delta\psi(w)\delta\bar{\psi}(v)}.$$

Including this result Eq. (124) takes the form

$$\begin{aligned}\frac{\delta S(x,y;[A^a_\mu])}{i\delta J^a_\mu(x)} &= \int d^4z \frac{\delta A^\nu_b(z)}{i\delta J^\mu_A(x)}\frac{\delta}{\delta A^\nu_b(z)}\left(\frac{\delta^2\Gamma}{\delta\psi(x)\delta\bar{\psi}(y)}\Big|_{\psi=0=\bar{\psi}}\right)^{-1} \\ &= \int d^4z d^4w d^4v \frac{\delta A^\nu_b(z)}{i\delta J^\mu_A(x)} \;\; S(x,w,[A^a_\mu])\Gamma^b_\nu(w,v,z)S(v,y,[A^a_\mu]). \qquad (132)\end{aligned}$$

Finally we compute

$$\frac{\delta A^\nu_b(z)}{i\delta J^\mu_a(x)} = -\frac{\delta^2 W}{i\delta J^\mu_a(x)\delta J^\nu_b(z)} = \left(\frac{\delta^2\Gamma}{i\delta A^\mu_a(x)\delta A^\nu_b(z)}\right)^{-1} =: D^{\mu\nu}_{ab}(x,z), \qquad (133)$$

where we defined the gluon propagator $D^{\mu\nu}_{ab}$. The result is then

$$\frac{\delta S(x,y;[A^a_\mu])}{i\delta J^a_\mu(x)} = \;\; = \int d^4w d^4v \;\; D^{\mu\nu}_{ab}(x,z)S(x,w)\Gamma^b_\nu(w,v,z)S(v,y). \qquad (134)$$

Now we can write the Dyson-Schwinger equation in the form

$$\begin{aligned}\delta^4(x-y) &= \left(\not\partial_x - \gamma_4\mu - m\right)S(x,y) + \\ &\quad \int d^4z d^4w d^4v \;\; ig\gamma^\mu t_a D^{\mu\nu}_{ab}(x,z)S(x,w)\Gamma^b_\nu(w,v,z)S(v,y) \qquad (135)\\ &= \int d^4v \left[\left(\not\partial_x - \gamma_4\mu - m\right)\delta^4(x-v) + \right. \\ &\quad \left. ig\int d^4w d^4z \;\; \gamma^\mu t_a D^{\mu\nu}_{ab}(x,z)S(x,w)\Gamma^b_\nu(w,v,z)\right]S(v,y). \qquad (136)\end{aligned}$$

Defining the proper quark self-energy

$$\Sigma(x,y) = ig\int d^4w d^4z \;\gamma^\mu t_a D^{\mu\nu}_{ab}(x,z)S(x,w)\Gamma^b_\nu(w,v,z), \qquad (137)$$

we arrive at the final form of the DSE:

$$\delta^4(x-y) = \int d^4v \left[\left(\not\partial_x - \gamma_4\mu - m\right)\delta^4(x-v) + \Sigma(x,v)\right]S(v,y). \qquad (138)$$

C Analytical calculations

We present some analytical results that are being used in section 3. The calculations require the gap function being parametrized as in section 3. Therefore, the results presented here must not be used in section 4.

C.1 Getting the quark propagator

The inverse full quark propagator is given by (cf. Eq. (55)),

$$(S^+)^{-1} = Z_2(S_0^+)^{-1} + Z_{1F}\Sigma^+ - Z_{1F}^2\Phi^- \left[Z_2(S_0^-)^{-1} + Z_{1F}\Sigma^-\right]^{-1}\Phi^+$$

using the identity in Eq. (80) this simplifies to

$$(S^+)^{-1} = Z_2(S_0^+)^{-1} + Z_{1F}\Sigma^+ - \left[Z_2(S_0^-)^{-1} + Z_{1F}\Sigma^-\right] Z_2^2 \sum_{e=\pm} |\phi_e(p)|^2 L_{\vec{p}}\Lambda_{\hat{p}}^{-e}$$

pulling out a factor of $Z_2(S_0^-)^{-1} + Z_{1F}\Sigma^-$ we get

$$\begin{aligned}(S^+)^{-1} &= \left[Z_2(S_0^-)^{-1} + Z_{1F}\Sigma^-\right]^{-1} \cdot \\ &\quad \left\{\left[Z_2(S_0^+)^{-1} + Z_{1F}\Sigma^+\right]\left[Z_2(S_0^-)^{-1} + Z_{1F}\Sigma^-\right] - Z_2^2\sum_{e=\pm}|\phi_e(p)|^2 L_{\vec{p}}\Lambda_{\hat{p}}^{-e}\right\}\end{aligned}$$

now we write the factors of the first term in curly brackets in terms of energy projectors to arrive at the form

$$\begin{aligned}&Z_2^2\left[Z_2(S_0^-)^{-1} + Z_{1F}\Sigma^-\right]^{-1} \cdot \sum_{e=\pm}\left\{\sum_{e'=\pm}(-1)\left[-e|\vec{p}|(1+\Sigma_A(p)) - i\omega_{\vec{p}}(1+\Sigma_C(p))\right]\right. \\ &\left.\left[-e'|\vec{p}|(1+\Sigma_A^*(p)) + i\omega_{\vec{p}}^*(1+\Sigma_C^*(p))\right] - |\phi_e(p)|^2 L_{\vec{p}}\right\}\gamma_4\Lambda_{\hat{p}}^{-e}\gamma_4\Lambda_{\hat{p}}^{e'} \\ = \;& -Z_2^2\left[Z_2(S_0^-)^{-1} + Z_{1F}\Sigma^-\right]^{-1} \cdot \sum_{e=\pm}\left\{\sum_{e'=\pm}\left[-e|\vec{p}|(1+\Sigma_A(p)) - i\omega_{\vec{p}}(1+\Sigma_C(p))\right]\right. \\ &\left.\left[-e'|\vec{p}|(1+\Sigma_A^*(p)) + i\omega_{\vec{p}}^*(1+\Sigma_C^*(p))\right] + |\phi_e(p)|^2 L_{\vec{p}}\right\}\Lambda_{\hat{p}}^{-e}\delta_{e,e'} \\ = \;& -Z_2^2\left[Z_2(S_0^-)^{-1} + Z_{1F}\Sigma^-\right]^{-1} \cdot \\ &\sum_{e=\pm}\left\{|e|\vec{p}|(1+\Sigma_A(p)) + i\omega_{\vec{p}}(1+\Sigma_C(p))| + |\phi_e(p)|^2 L_{\vec{p}}\right\}\Lambda_{\hat{p}}^{-e}.\end{aligned}$$

As a last step we use the fact that the matrix $L_{\vec{p}}$ can be written in terms of projectors $\mathcal{P}_{\vec{p}}^r$ and that the sum of the projectors is the identity matrix.

$$\begin{aligned}(S^+)^{-1} &= -Z_2^2\left[Z_2(S_0^-)^{-1} + Z_{1F}\Sigma^-\right]^{-1} \cdot \\ &\quad \sum_{e=\pm,r}\left\{|e|\vec{p}|(1+\Sigma_A(p)) + i\omega_{\vec{p}}(1+\Sigma_C(p))| + \lambda_r|\phi_e(p)|^2\right\}\mathcal{P}_{\vec{p}}^r\Lambda_{\hat{p}}^{-e}.\end{aligned} \tag{139}$$

The inverse full quark propagator is then easily inverted:

$$\begin{aligned} S^{+}(p) &= -\frac{1}{Z_2^2}\left[Z_2(S_0^-)^{-1}+Z_{1F}\Sigma^-\right] \\ &\quad \sum_{e=\pm,r}\frac{\mathcal{P}^r_{\vec{p}}\Lambda^{-e}_{\hat{p}}}{|e|\vec{p}|(1+\Sigma_{A,r}(p))+i\omega_p(1+\Sigma_{C,r}(p))|^2+\lambda_r\left|\phi_e(p)\right|^2}. \end{aligned} \tag{140}$$

Another identity that we used in this work is derived here. It is very straightforward to compute.

$$\begin{aligned} &\left[Z_2(S_0^-)^{-1}+Z_{1F}\Sigma^-\right]^{-1}\Phi^+\left[Z_2(S_0^-)^{-1}+Z_{1F}\Sigma^-\right]= \\ &\frac{Z_2}{Z_{1F}}\sum_{e,e',e''}\frac{e|\vec{p}|(1+\Sigma_A(p))+i\omega_{\vec{p}}(1+\Sigma_C(p))}{e''|\vec{p}|(1+\Sigma_A(p))+i\omega_{\vec{p}}(1+\Sigma_C(p))}\phi_{e'}(p)(\gamma_4\Lambda^{e}_{\hat{p}})^{-1}\mathcal{M}_{\vec{p}}\Lambda^{e'}_{\hat{p}}\gamma_4\Lambda^{e''}_{\hat{p}}= \\ &\frac{Z_2}{Z_{1F}}\sum_{e,e',e''}\frac{e|\vec{p}|(1+\Sigma_A(p))+i\omega_{\vec{p}}(1+\Sigma_C(p))}{e''|\vec{p}|(1+\Sigma_A(p))+i\omega_{\vec{p}}(1+\Sigma_C(p))}\phi_{e'}(p)\gamma_4\Lambda^{-e}_{\hat{p}}\Lambda^{e'}_{\hat{p}}\mathcal{M}_{\vec{p}}\gamma_4\delta_{e',-e''}= \\ &\frac{Z_2}{Z_{1F}}\sum_{e,e',e''}\frac{e|\vec{p}|(1+\Sigma_A(p))+i\omega_{\vec{p}}(1+\Sigma_C(p))}{e''|\vec{p}|(1+\Sigma_A(p))+i\omega_{\vec{p}}(1+\Sigma_C(p))}\phi_{e'}(p)\gamma_4\mathcal{M}_{\vec{p}}\Lambda^{e'}_{\hat{p}}\gamma_4\delta_{e',-e''}\delta_{e',-e}= \\ &\frac{Z_2}{Z_{1F}}\sum_{e'}\left[\phi_{e'}(p)\right]\gamma_4\mathcal{M}_{\vec{p}}\gamma_4\Lambda^{-e'}_{\hat{p}}. \end{aligned}$$

C.2 Calculating the effective action

To compute the effective action we have to perform some manipulations on the general formula, Eq. (95),

$$\mathcal{A}[\mathcal{S}]=-\frac{1}{2}\mathrm{Tr}_{p,D,c,f,N}[\mathrm{Ln}\mathcal{S}^{-1}]+\frac{1}{4}\mathrm{Tr}_{p,D,c,f,N}[1-\mathcal{S}_0^{-1}\mathcal{S}], \tag{141}$$

such that we can actually compute the value of the effective action. The first step is to do the trace over Nambu-Gor'kov space.
Two commonly known identities will be used, they are

$$\mathrm{Tr}[\mathrm{Log}[M]]=\log[\mathrm{Det}[M]] \qquad \mathrm{Det}\begin{pmatrix} A & B \\ C & D\end{pmatrix}=AD-BD^{-1}CD,$$

where A, B, C, D and M are arbitrary matrices. With this identity at hand, we can do the trace over Nambu-Gor'kov space to get:

$$\begin{aligned} \mathcal{A}[\mathcal{S}] &= -\frac{1}{2}\mathrm{Tr}_{p,D,c}[\mathrm{Ln}\left\{[\,(S_0^+)^{-1}(p)+\Sigma^+(p)][\,(S_0^-)^{-1}(p)+\Sigma^-(p)]\right. \\ &\quad \left.-\Phi^-(p)[(S_0^-)^{-1}(p)+\Sigma^-(p)]^{-1}\Phi^+(p)[(S_0^-)^{-1}(p)+\Sigma^-(p)]\right\}] \\ &\quad +\frac{1}{4}\mathrm{Tr}_{p,D,c}\left[2-S^+(p)(S_0^+)^{-1}(p)-S^-(p)(S_0^-)^{-1}(p)\right] \end{aligned} \tag{142}$$

The first term in Eq. (142) can be further evaluated. Therefore, we will express the quark propagators, the selfenergies and the gap functions with the help of energy projectors and the projectors $\mathcal{P}^r_{\hat{p}}$. We will also make use of Eq. (80).

$$
\begin{aligned}
& -\mathrm{Tr}_{p,D,c}\left[\mathrm{Ln}\left\{[\ (S_0^+)^{-1}(p)+\Sigma^+(p)][\ (S_0^-)^{-1}(p)+\Sigma^-(p)]\right.\right. \\
& \left.\left. -\Phi^-(p)[(S_0^-)^{-1}(p)+\Sigma^-(p)]^{-1}\Phi^+(p)[(S_0^-)^{-1}(p)+\Sigma^-(p)]\right\}\right] \\
= \quad & -\mathrm{Tr}_{p,D,c}\left[\mathrm{Ln}\left\{(\ (S_0^+)^{-1}(p)+\Sigma^+(p))((S_0^-)^{-1}(p)+\Sigma^-(p))-\sum_{e=\pm}|\phi^e|^2 L_{\vec{p}}\Lambda^{-e}_{\hat{p}}\right\}\right] \\
= \quad & -\mathrm{Tr}_{p,D,c}\left[\mathrm{Ln}\left\{-\sum_{e=\pm,r}\left\{|e|\vec{p}|(1+\Sigma_A(p)+i\omega_p(1+\Sigma_C(p))|^2\mathcal{P}^r_{\hat{p}}+|\phi^e|^2 L_{\vec{p}}\right\}\Lambda^{-e}_{\hat{p}}\right\}\right] \\
= \quad & -\mathrm{Tr}_{p,D,c}\left[\mathrm{Ln}\left\{-\sum_{e=\pm,r}\left\{|e|\vec{p}|(1+\Sigma_A(p)+i\omega_p(1+\Sigma_C(p))|^2+\lambda_r|\phi^e|^2\right\}\mathcal{P}^r_{\hat{p}}\Lambda^{-e}_{\hat{p}}\right\}\right] \\
= \quad & -\mathrm{Tr}_p\left[\sum_{e=\pm,r}\mathrm{Ln}\left[-|e|\vec{p}|(1+\Sigma_A(p)+i\omega_p(1+\Sigma_C(p))|^2-\lambda_r|\phi^e|^2\right]\mathrm{Tr}_{D,c}[\mathcal{P}^r_{\hat{p}}\Lambda^{-e}_{\hat{p}}]\right] \qquad (143)
\end{aligned}
$$

The remaining traces over colour and Dirac space can easily be evaluated. The minus sign in the logarithm might seem spurious. However, this is not a problem since we will eventually take the difference between two logarithms of this type. Doing so, the minus sign is cancels out.
The second term in Eq. (142) can also be simplified by noticing that

$$
\begin{aligned}
\mathrm{Tr}[(S_0^-)^{-1}(p)S^-(p)] &= \mathrm{Tr}[(C(S_0^+(-p))^T C)^{-1}C(S^+(-p))^T C] \qquad (144)\\
&= \mathrm{Tr}[CC^{-1}((S_0^+(-p))^T)^{-1}C^{-1}C(S^+(-p))^T] \\
&= \mathrm{Tr}[((S_0^+(-p))^T)^{-1}(S^+(-p))^T] \\
&= \mathrm{Tr}[((S_0^+(-p))^{-1}S^+(-p))^T] \\
&= \mathrm{Tr}[(S_0^+(-p))^{-1}S^+(-p)]. \qquad (145)
\end{aligned}
$$

This allows us to use only the quasiparticle propagator. $\mathrm{Tr}[(S_0^+(p))^{-1}S^+(p)]$ is easily evaluated

$$
\begin{aligned}
&\mathrm{Tr}[(S_0^+(p))^{-1}S^+(p)] = \\
&\sum_{e',e=\pm,r}\frac{-[e'|\vec{p}|+i\omega_p][-e|\vec{p}|(1+\Sigma_A^*(p))+i\omega_p^*(1+\Sigma_C^*(p))]}{|e|\vec{p}|(1+\Sigma_A(p))+i\omega_p(1+\Sigma_C(p))|^2+\lambda_r|\phi_e(p)|^2}\mathrm{Tr}_{D,c}[\gamma_4\Lambda^{e'}_{\hat{p}}\gamma_4\mathcal{P}^r_{\vec{p}}\Lambda^{-e}_{\hat{p}}] \\
&\sum_{e=\pm,r}\frac{[e|\vec{p}|-i\omega_p][e|\vec{p}|(1+\Sigma_A^*(p))-i\omega_p^*(1+\Sigma_C^*(p))]}{|e|\vec{p}|(1+\Sigma_A(p))+i\omega_p(1+\Sigma_C(p))|^2+\lambda_r\,|\phi_e(p)|^2}\mathrm{Tr}_{D,c}[\mathcal{P}^r_{\vec{p}}\Lambda^{-e}_{\hat{p}}]. \qquad (146)
\end{aligned}
$$

Here we used $\gamma_4\Lambda^e_{\hat{p}}=\Lambda^{-e}_{\hat{p}}\gamma_4$ and $\Lambda^e_{\hat{p}}\Lambda^{e'}_{\hat{p}}=\Lambda^e_{\hat{p}}\delta_{ee'}$. This can now easily be implemented. Left to do is only evaluating the traces over colour and Dirac space for $\mathcal{P}^r_{\vec{p}}\Lambda^{-e}_{\hat{p}}$. The results are, where we used that the dependence on e in $\mathrm{Tr}_{D,c}[\mathcal{P}^r_{\vec{p}}\Lambda^{-e}_{\hat{p}}]$ drops out,

	transverse phase	mixed phase
r = 1	6	4
r = 2	0	2

D Numerical methods

D.1 Integration in hyperspherical coordinates

Any arbitrary momentum P is parametrised in hyperspherical coordinates by

$$\begin{pmatrix} P_1 \\ P_2 \\ P_3 \\ P_4 \end{pmatrix} = \begin{pmatrix} P\sin\chi\sin\theta\sin\phi \\ P\sin\chi\sin\theta\cos\phi \\ P\sin\chi\cos\theta \\ P\cos\chi \end{pmatrix}, \tag{147}$$

where ϕ should not be confused with the gap functions. An integral over all momenta is then given by

$$\int \frac{d^4p}{(2\pi)^4} = \frac{1}{(2\pi)^4}\int_0^\infty dp\; p^3 \int_0^{2\pi} d\phi \int_0^\pi d\theta \sin\theta \int_0^\pi d\chi \sin^2\chi \tag{148}$$

Since we are only dealing with two momenta p and q in our equations we are quite free to choose our coordinate system. p is the external quark momentum and q is the quark loop momentum.

Zero density

One calculation at zero density is needed for renormalisation. In this calculation we will use $O(4)$-invariance to choose the coordinate system in a way such that the external quark momentum p is purely timelike and the loop momentum q has only 3,4-components

$$p^\mu = \begin{pmatrix} p_1 \\ p_2 \\ p_3 \\ p_4 \end{pmatrix} = \begin{pmatrix} 0 \\ 0 \\ 0 \\ p \end{pmatrix} \quad , \quad q^\mu = \begin{pmatrix} q_1 \\ q_2 \\ q_3 \\ q_4 \end{pmatrix} = \begin{pmatrix} 0 \\ 0 \\ q\sin\chi \\ q\cos\chi \end{pmatrix}. \tag{149}$$

In this case the integration over ϕ and θ is trivial, it simply gives a factor of 4π.

Nonzero density

At nonzero density the situation is more involved since the 4-axis is distinguished due to the chemical potential. The diquark condensate in the CSL phase is $SO(3)$-symmetric and thus does not introduce additional difficulties. We thus choose the momenta

$$p^\mu = \begin{pmatrix} p_1 \\ p_2 \\ p_3 \\ p_4 \end{pmatrix} = \begin{pmatrix} 0 \\ 0 \\ p\sin\chi_p \\ p\cos\chi_p \end{pmatrix} \quad , \quad q^\mu = \begin{pmatrix} q_1 \\ q_2 \\ q_3 \\ q_4 \end{pmatrix} = \begin{pmatrix} 0 \\ q\sin\chi_q\sin\theta_q \\ q\sin\chi_q\cos\theta_q \\ q\cos\chi_q \end{pmatrix}. \tag{150}$$

D.2 Numerical Integration

We use a simple Riemann quadrature however we use an integration grid that is not uniform. We manually assign more points to momentum areas that are most relevant to the solution.

Momentum Integrals

We only integrate from the infrared cutoff Λ_{IR} to the ultraviolet cutoff Λ_{UV}. As these quantities differ by many orders of magnitude and we expect the most important contributions to the integrals to come from the momentum region around the chemical potential, we distribute the integration points for the momentum integrals logarithmically. This is done via a transformation $q = e^{q'}$ and we get

$$\int_{\Lambda_{IR}}^{\Lambda_{UV}} dq q^3 f(q) = \int_{\ln \Lambda_{IR}}^{\ln \Lambda_{UV}} dq' e^{q'} \; e^{3q'} f(e^{q'}) = \int_{\ln \Lambda_{IR}}^{\ln \Lambda_{UV}} dq' e^{4q'} f(e^{q'}). \tag{151}$$

If $x_{i,j}$ and $w_{i,j}$ are the abscissas and weights for the Riemann integration this becomes

$$\int_{\Lambda_{IR}}^{\Lambda_{UV}} dq q^3 f(q) = \sum_{i,j} w_{i,j} e^{4x_{i,j}} f(e^{x_{i,j}}), \tag{152}$$

we used double indices to account for the use of non-uniform integration areas. This means we subdivide the whole momentum range into areas with a specific upper and lower bound for the values of momentum q and the angle with the 4-axis χ_q. An example is shown in Fig. 27

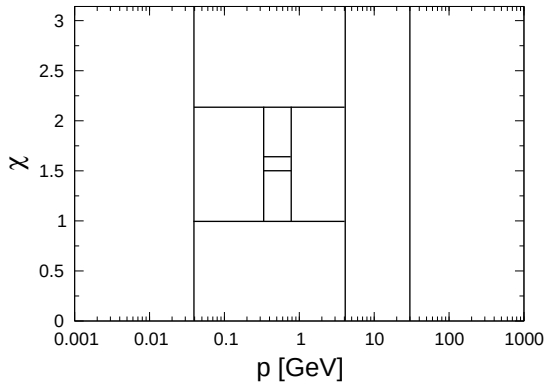

Figure 27: An example for the integration areas. Lines show the integration area boundaries

Angular integrals

We have three angular integrals $\int_0^{2\pi} d\phi, \int_0^{\pi} d\theta \sin\theta, \int_0^{\pi} d\chi \sin^2\chi$. The integral over ϕ can always be performed analytically and trivially yields 2π as result, because none of the integrands depend on ϕ.
For the other two integrals we again use Riemann quadrature and denote the weights and

abscissas for the χ/θ-integration by $w^{\chi}_{i,j}/w^{\theta}_{i}$ and $\chi_{i,j}/\theta_i$:

$$\int_0^{\pi} d\theta \sin\theta = \sum_i w_i^{\theta} \sin(\theta_i) \tag{153}$$

$$\int_0^{\pi} d\chi \sin^2\chi = \sum_{i,j} w_{i,j}^{\chi} \sin^2(\chi_{i,j}). \tag{154}$$

For the θ-integration we only use one single set of weights and abscissas, except for the high-momentum region where we perform a special treatment of the gluon pole $1/k^2$.

Solving the gap equation numerically

The gap equation is solved numerically within an iterative procedure. We assume that the equation has at least one fixed point such that $F(\Phi) = \Phi$ where $F(\Phi)$ is the integral expression on the right hand side of Eq. (61).

D.3 Code generation

In the fully selfconsistent ansatz for the CSL phase we deal with large (12×12) matrices that contain entries of up to 20 different functions. For example to get the anomalous propagator we have to multiply three different of these matrices and extract the individual structures that correspond to the parametrisation of the anomalous propagator. The effort needed to do this requires the use of an automated routine. Fortunately all we need is available in the computer mathematics system *Mathematica*. Here we are going to outline the steps made to build program that can solve the DSE for the quark propagator in the CSL phase.
First we define the Euclidian Dirac gamma matrices and the antisymmetric Gell-Mann matrices in Mathematica. Now we have to define a Kronecker product this is done by the prescription to put the Dirac matrices at the position where the entries in the Gell-Mann matrices would reside. Here is an example:

$$\begin{pmatrix} \alpha & \beta \\ \gamma & \delta \end{pmatrix} \otimes \begin{pmatrix} a & b & c \\ d & e & f \\ g & h & i \end{pmatrix} = \begin{pmatrix} \alpha a & \alpha b & \alpha c & \beta a & \beta b & \beta c \\ \alpha d & \alpha e & \alpha f & \beta d & \beta e & \beta f \\ \alpha g & \alpha h & \alpha i & \beta g & \beta h & \beta i \\ \gamma a & \gamma b & \gamma c & \delta a & \delta b & \delta c \\ \gamma d & \gamma e & \gamma f & \delta d & \delta e & \delta f \\ \gamma g & \gamma h & \gamma i & \delta g & \delta h & \delta i \end{pmatrix}. \tag{155}$$

This example was only with 2×2 and 3×3 matrices but the generalisation is obvious. The product of two objects that are Kronecker products of matrices in colour and Dirac space is now a simple matrix multiplication.
Now all we have to do is define all the quantities needed in the calculation, implement the relations amongst each other and extract the scalar equations for the ansatz functions out of the matrix equations. This procedure is different for the two different ansätze.
In the first case, used in section 3, we could perform most of the calculation analytically

and thus do not have to resort extensively to computer algebra. For the fully selfconsistent CSL analytic calculations are to tedious to be done. Therefore, we had to resort to numerical algorithms to invert propagators and to compute the integration kernels. To get the algebraic expressions we used Mathematica.

References

[1] J. C. Collins and M. J. Perry, "SUPERDENSE MATTER: NEUTRONS OR ASYMPTOTICALLY FREE QUARKS?," *Phys. Rev. Lett.* **34** (1975) 1353.

[2] B. C. Barrois, "SUPERCONDUCTING QUARK MATTER," *Nucl. Phys.* **B129** (1977) 390.

[3] D. Bailin and A. Love, "SUPERFLUIDITY AND SUPERCONDUCTIVITY IN RELATIVISTIC FERMION SYSTEMS," *Phys. Rept.* **107** (1984) 325.

[4] M. G. Alford, K. Rajagopal, and F. Wilczek, "QCD at finite baryon density: Nucleon droplets and color superconductivity," *Phys. Lett.* **B422** (1998) 247–256, `hep-ph/9711395`.

[5] R. Rapp, T. Schafer, E. V. Shuryak, and M. Velkovsky, "Diquark Bose condensates in high density matter and instantons," *Phys. Rev. Lett.* **81** (1998) 53–56, `hep-ph/9711396`.

[6] R. Rapp, T. Schäfer, E. V. Shuryak, and M. Velkovsky, "High-density QCD and instantons," *Annals Phys.* **280** (2000) 35–99, `hep-ph/9904353`.

[7] D. Blaschke and C. D. Roberts, "Deconfinement and hadron properties at extremes of temperature and density," *Nucl. Phys.* **A642** (1998) 197–209, `nucl-th/9807008`.

[8] M. G. Alford, "Color superconducting quark matter," *Ann. Rev. Nucl. Part. Sci.* **51** (2001) 131–160, `hep-ph/0102047`.

[9] M. Buballa, "NJL model analysis of dense quark matter," *Phys. Rept.* **407** (2005) 205–376, `hep-ph/0402234`.

[10] A. Schmitt, "The ground state in a spin-one color superconductor," *Phys. Rev.* **D71** (2005) 054016, `nucl-th/0412033`.

[11] S. B. Rüster, V. Werth, M. Buballa, I. A. Shovkovy, and D. H. Rischke, "The phase diagram of neutral quark matter: Self-consistent treatment of quark masses," *Phys. Rev.* **D72** (2005) 034004, `hep-ph/0503184`.

[12] D. Blaschke, S. Fredriksson, H. Grigorian, A. M. Oztas, and F. Sandin, "The phase diagram of three-flavor quark matter under compact star constraints," *Phys. Rev.* **D72** (2005) 065020, `hep-ph/0503194`.

[13] K. Rajagopal and F. Wilczek, "The condensed matter physics of QCD," `hep-ph/0011333`.

[14] M. Alford and K. Rajagopal, "Absence of two-flavor color superconductivity in compact stars," *JHEP* **06** (2002) 031, `hep-ph/0204001`.

[15] H. Grigorian, D. Blaschke, and D. Voskresensky, "Cooling of neutron stars with color superconducting quark cores," *Phys. Rev.* **C71** (2005) 045801, astro-ph/0411619.

[16] A. Schmitt, "Spin-one color superconductivity in cold and dense quark matter," nucl-th/0405076.

[17] D. N. Aguilera, D. Blaschke, M. Buballa, and V. L. Yudichev, "Color-spin locking phase in two-flavor quark matter for compact star phenomenology," *Phys. Rev.* **D72** (2005) 034008, hep-ph/0503288.

[18] J. I. Kapusta, "FINITE TEMPERATURE FIELD THEORY,". Cambridge University Press, Cambridge, 1989.

[19] A. Höll, C. D. Roberts, and S. V. Wright, "Hadron physics and Dyson-Schwinger equations," nucl-th/0601071.

[20] A. Höll, C. D. Roberts, and S. V. Wright, "A perspective on hadron physics," nucl-th/0604029.

[21] C. S. Fischer and R. Alkofer, "Non-perturbative propagators, running coupling and dynamical quark mass of Landau gauge QCD," *Phys. Rev.* **D67** (2003) 094020, hep-ph/0301094.

[22] M. S. Bhagwat, M. A. Pichowsky, C. D. Roberts, and P. C. Tandy, "Analysis of a quenched lattice-QCD dressed-quark propagator," *Phys. Rev.* **C68** (2003) 015203, nucl-th/0304003.

[23] D. Nickel, J. Wambach, and R. Alkofer, "Color-superconductivity in the strong-coupling regime of Landau gauge QCD," *Phys. Rev.* **D73** (2006) 114028, hep-ph/0603163.

[24] M. Le Bellac, "Thermal Field Theory,". Cambridge University Press, Cambridge, 1996.

[25] J. Bardeen, L. N. Cooper, and J. R. Schrieffer, "Theory of superconductivity," *Phys. Rev.* **108** (1957) 1175–1204.

[26] Y. Nambu, "Quasi-particles and gauge invariance in the theory of superconductivity," *Phys. Rev.* **117** (1960) 648–663.

[27] D. H. Rischke, "The quark-gluon plasma in equilibrium," *Prog. Part. Nucl. Phys.* **52** (2004) 197–296, nucl-th/0305030.

[28] M. G. Alford, J. A. Bowers, J. M. Cheyne, and G. A. Cowan, "Single color and single flavor color superconductivity," *Phys. Rev.* **D67** (2003) 054018, hep-ph/0210106.

[29] T. Schäfer, "Quark hadron continuity in QCD with one flavor," *Phys. Rev.* **D62** (2000) 094007, hep-ph/0006034.

[30] R. D. Pisarski and D. H. Rischke, "Color superconductivity in weak coupling," *Phys. Rev.* **D61** (2000) 074017, nucl-th/9910056.

[31] H. Abuki, T. Hatsuda, and K. Itakura, "Structural change of Cooper pairs and momentum-dependent gap in color superconductivity," *Phys. Rev.* **D65** (2002) 074014, hep-ph/0109013.

[32] T. A. Lasinski *et al.*, "Review of particle properties. particle data group," *Rev. Mod. Phys.* **45** (1973) S1–S175.

[33] A. Schmitt, I. A. Shovkovy, and Q. Wang, "Neutrino emissivity from spin-one color superconductors," *PoS* **JHW2005** (2006) 028.

[34] R. Alkofer and L. von Smekal, "The infrared behavior of QCD Green's functions: Confinement, dynamical symmetry breaking, and hadrons as relativistic bound states," *Phys. Rept.* **353** (2001) 281, hep-ph/0007355.

[35] C. D. Roberts and S. M. Schmidt, "Dyson-Schwinger equations: Density, temperature and continuum strong QCD," *Prog. Part. Nucl. Phys.* **45** (2000) S1–S103, nucl-th/0005064.

Acknowledgements

First of all I would like to thank Professor Wambach for giving me the opportunity to work on this subject. In addition, I would like to thank him for the possibility to visit several conferences and schools, which considerably broadened my perspective in physics.

I would also like to thank Dr. Michael Buballa for interesting discussions and his interest in my work.

Special thanks go to Dominik Nickel who introduced me into the subject and was always there to help me. I also appreciate his patience to discuss even the slightest technical detail with me, as well as bigger, more conceptual problems. Due to his guidance I learnt a lot.

I thank the NHQ and TNP groups at Darmstadt University of Technology for an enjoyable working atmosphere. For carefully reading the manuscript my thanks go to Haris Djapo, Felix Schmitt and Verena Werth. Mathias Wagner and Professor Robert Roth deserve a special thank for computer administration and support.

Not directly involved but nevertheless equally important are the friends that accompanied me throughout the last years and made me the person I am. Ilja Buchmüller, Michael Elvers, Frank Harlacher, Liv Holzwarth, Ulrich Jäger, Florian Kaufhold, Judith Krietsch, Marcel Labrenz, Johannes Ling, Marcus Major, Wolfgang Müller, Lars Orth and Viola Priesemann.

My special gratefullness goes to my family that has always been there for me and supported me the best they could. Without them I would not be able to write these words.

Erklärung zur Diplomarbeit gemäß §19 Abs. 6 DPO/AT

Hiermit versichere ich, die Diplomarbeit ohne Hilfe Dritter nur mit den angegebenen Quellen und Hilfsmitteln angefertigt zu haben. Alle Stellen, die aus di esen Quellen entnommen wurden, sind als solche kenntlich gemacht worden. Diese Arbeit hat in gleicher oder ähnlicher Form noch keiner Prüfungsbehörde vorgelegen.

Darmstadt, den 29.08.2006

Marc Florian Marhauser